NASA/CR-1998-208730

Numerical Stability and Control Analysis Towards Falling-Leaf Prediction Capabilities of Splitflow for Two Generic High-Performance Aircraft Models

Eric F. Charlton
Lockheed-Martin Tactical Aircraft Systems, Fort Worth, Texas

National Aeronautics and
Space Administration

Langley Research Center
Hampton, Virginia 23681-2199

Prepared for Langley Research Center
under Contract NAS1-96014

September 1998

Available from:

NASA Center for AeroSpace Information (CASI)
7121 Standard Drive
Hanover, MD 21076-1320
(301) 621-0390

National Technical Information Service (NTIS)
5285 Port Royal Road
Springfield, VA 22161-2171
(703) 605-6000

Numerical Stability and Control Analysis Towards Falling-Leaf Prediction Capabilities of *Splitflow* for Two Generic High-Performance Aircraft Models

Eric F. Charlton
Lockheed Martin
Tactical Aircraft Systems

Abstract

Aerodynamic analyses are performed using the Lockheed Martin Tactical Aircraft Systems (LMTAS) *Splitflow* computational fluid dynamics code to investigate the computational prediction capabilities for vortex-dominated flow fields of two different tailless aircraft models at large angles of attack and sideslip. These computations are performed with the goal of providing useful stability and control data to designers of high-performance aircraft. Appropriate metrics for accuracy, time, and ease of use are determined in consultation with both the LMTAS Advanced Design and Stability and Controls groups. Results are obtained and compared to wind tunnel data for all six forces and moments. Moment data is combined to form a "falling leaf" stability analysis. Finally, a handful of viscous simulations were also performed to further investigate nonlinearities and possible viscous effects in the differences between the accumulated inviscid computational and experimental data.

Contents

List of Figures

List of Tables

1 Nomenclature

Parameters:

α angle of attack, usually in degrees.

β sideslip angle, usually in degrees.

λ wing sweep angle, usually in degrees.

t/c wing thickness to chord ratio, usually in percent.

Variables:

C_{l_β} lateral stability derivative, $\partial C_l/\partial\beta$ (Section 7).

C_{n_β} directional stability derivative, $\partial C_n/\partial\beta$ (Section 7).

$C_{n_{\beta_{\mathrm{DYN}}}}$ Dutch-roll stability parameter (Section 7).

F_x, F_y, F_z force coefficients in the body x-, y-, and $z-$axis respectively, also referred to as C_A, C_Y, and C_N respectively.

I_{xx}, I_{zz}, I_{xz} moments of inertia about the x-, z-, and x/z axes respectively.

M_x, M_y, M_z moment coefficients around the body x-, y-, and $z-$axis respectively, also referred to as C_l, C_m, C_n or CLLB, CLM, CLNB ("C little L body," "C little M," and "C little N body," where "body" refers to the reference axis).

SRYP synchronous roll-yaw parameter (Section 7).

$\vec{v}$ velocity, (u, v, w) in body axes.

$\vec{\omega}$ vorticity $(\nabla \times \vec{v})$, in body axes.

Abbreviations:

BC boundary condition

CFD computational fluid dynamics

ICE LMTAS Innovative Control Effectors (tailless delta wing) model

LE leading edge

LaRC NASA Langley Research Center

LM Lockheed Martin

LMTAS Lockheed Martin, Tactical Aircraft Systems division

MTVI NASA Langley Modular Transonic Vortex Interaction aircraft model

PVM Parallel Virtual Machine library

RCS radar cross section

SARL Subsonic Aerodynamic Research Laboratory

S&C stability and controls

WT wind tunnel (in this report, usually SARL)

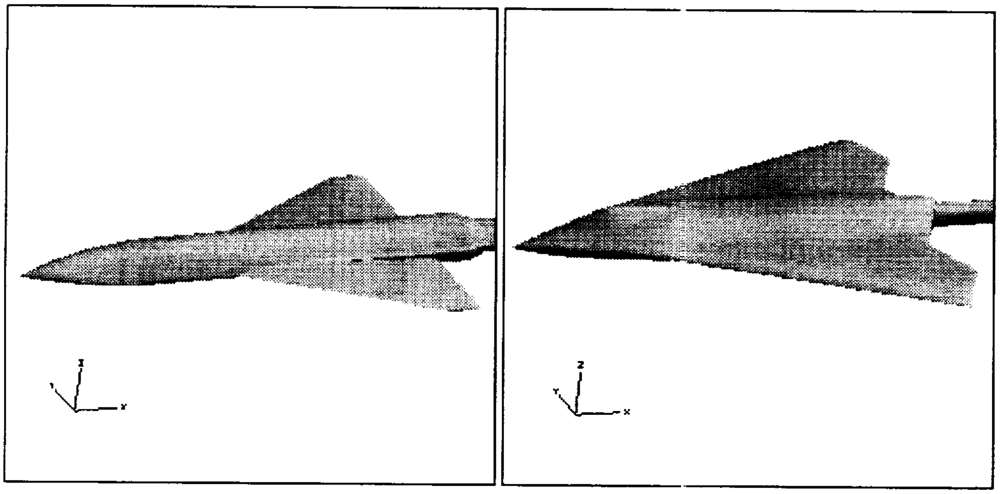

(a) MTVI (b) ICE

Figure 1: Baseline aircraft model configurations

2 Introduction

Aerodynamic design of high-performance aircraft requires detailed knowledge of the often-complicated airflow around the surface. High-performance aircraft usually make use of chines and surface blends between fuselages and wings to encourage vortex lift for maneuvering without sharp intersections between the wing and fuselage. Recent concerns regarding radar cross section (RCS, i.e. "stealth") have placed additional emphasis on sharp, well-defined surface intersections and are often leading to tailless aircraft designs.

The use of modified delta wings and sharp-edged leading edges often leads to vortex-dominated flows. The problem is further complicated by the large ranges of angle of attack (α) and sideslip (β) commonly experienced by tactical aircraft. The blended fuselage or chine along with the leading edge of the wing often creates multiple vortices which *interact* in complicated and highly-nonlinear manners.

The present study is part of the NASA Langley Research Center sponsored project (described in References 1–8) aimed at assessing the viability of using various state-of-the-art CFD Euler technology for efficient application of aerodynamic analysis during the preliminary design process. This work demonstrates how the LMTAS-developed Cartesian/unstructured grid method, the *Splitflow* code, can be used to rapidly analyze the flow around high-performance aircraft shapes and advance their design process. Results for the test cases are presented and measured with respect to runtime, accuracy, and the ease of use. In order for CFD to be used routinely in the design of high-performance aircraft, certain standards must be met for accuracy, time required, and ease of use.

3 Configuration

Two configurations were analyzed to provide comparison data for different types of aircraft, as shown in Figure 1. Each is a tailless delta wing aircraft model, but a different method is used in each to blend the wing and fuselage. In both cases, the flows are dominated by multiple interacting

β	α								
0		12		20		30		40	
2	6	12	16	20	25	30	35	40	45

Table 1: MTVI α/β-sweep (inviscid)

β	α									
0	0		10	15	20					30
5	0		10	15	20					30
10	0	5	10	15	20	22	24	26	28	30
20	0	5	10	15	20	22	24	26	28	30

Table 2: Tailless Delta (ICE) α-sweep (inviscid)

vortices. As these vortices interact, their influence on each other and the upper surface of the wing will set the corresponding aerodynamic performance of the vehicles. In each case, the key to a vortex-driven solution is resolving the vortex core. But adaption to the core can be tricky—at high α, vortex breakdown can become an important effect, and vortex breakdown is especially aggravated by high β.

The first configuration is the NASA Langley Modular Transonic Vortex Interaction (MTVI) model. MTVI is a delta wing with a long chined fuselage, as shown in Figure 1(a). At high α, vortices are created off of both the chine and the leading edge of the wing which interact as they pass over the upper surface of the aircraft model. The geometry and wind tunnel forces and moment data were provided by NASA Langley Research Center [9]. The MTVI cases computed are listed in Table 1.

The second configuration is the LMTAS tailless delta wing, referred to here (and in many earlier publications) as the Innovative Control Effectors (ICE) model. The ICE model has a blended fuselage and canopy, with a serrated ("broken") trailing edge. The ICE model also has very high camber with a very thin wing airfoil ($t/c = 4\%$), which caused difficulty during the grid generation phase as will be discussed later in Section 5.3. The ICE model is shown in Figure 1(b). Table 2 lists the cases performed for the sweeps across angle-of-attack, Table 3 lists the additional cases performed for the sweep across slip angle, and Table 4 lists the viscous cases that were added to investigate the possibility of viscous effects causing discrepancies between the inviscid solutions and the Subsonic Aerodynamic Research Laboratory (SARL) wind tunnel data.

4 Computational Resources

Two versions of the Lockheed Martin unstructured Cartesian code *Splitflow* were used for this analysis. The newer code, *Omnigrid Splitflow*, is a parallel code using Parallel Virtual Machine (PVM,

α	β							
20	2.5	5.0	7.5	10.0	12.5	15.0	17.5	20.0

Table 3: Tailless Delta (ICE) β-sweep (inviscid)

β	α		
10	22	24	28
20	22		28

Table 4: Tailless Delta (ICE), viscous

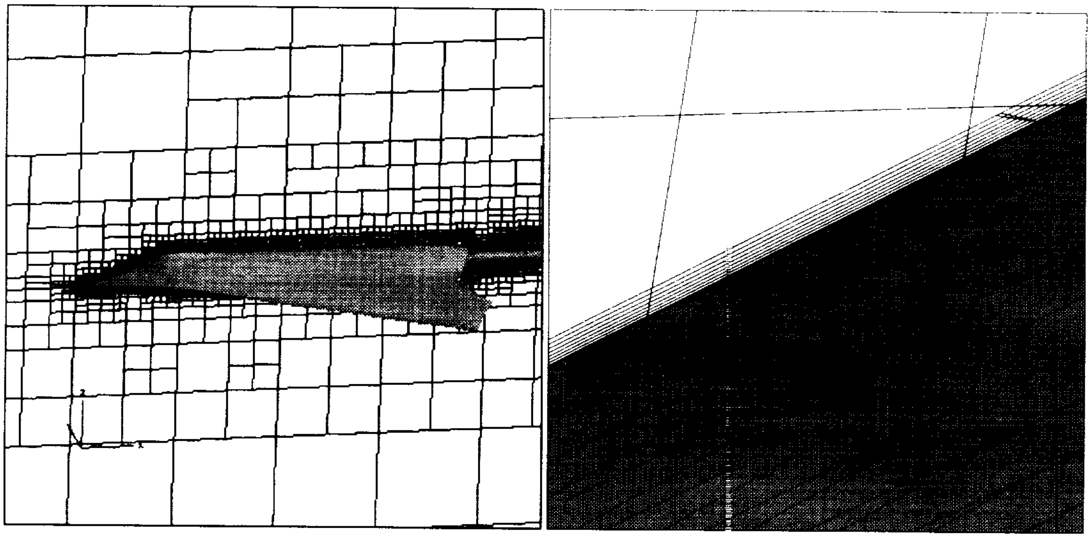

(a) Slice through an omnigrid

(b) Slice through a hybrid grid

Figure 2: Omnigrid and near-surface prismatic grid example on the body symmetry plane

described in [10]) that solves the Euler equations. *Hybrid Splitflow* is a vector code that was used to solve the Navier-Stokes equations. The parallel *Omnigrid* cases were computed on networks of SGI workstations, an HP 2000-series supercomputer, and LMTAS Cray J-90's. The vector computations were performed on the Cray J-90's. An example of an omnitree grid and the prismatic layer near the surface of a hybrid grid are shown in Figures 2(a) and 2(b) respectively.

Each version of *Splitflow* uses a tree-based data structure to build and store the grid. Computational grids are built by starting from a "root" cell and recursively refining one cell into smaller "children" grid cells. *Omnigrid Splitflow* yields additional efficiency by refining grid cells in each direction independently, yielding as few as two cells per cell refinement; the octree model used by *Hybrid Splitflow* yields a constant eight-children-per-parent cell refinement. Each code uses a finite-volume conservation scheme with an upwind flux formulation and has a preconditioner available for low Mach number flow solutions.

4.1 Inviscid

The inviscid simulations were computed with *Omnigrid Splitflow*. In practice, the directional cell splitting used by *Omnigrid Splitflow* can yield the same grid resolution as *Hybrid Splitflow* using approximately *half* the number of cells. *Omnigrid Splitflow* uses a pointwise semi-implicit time update with subiterations for more-efficient parallel computation.

Number of layers	9
Growth rate	1.1
Initial spacing	0.001

Table 5: ICE prismatic grid parameters

4.2 Viscous

The five viscous simulations were computed with *Hybrid Splitflow*. *Hybrid Splitflow* uses a prismatic grid grown from the surface in addition to the Cartesian octree grid. The prismatic grid is sized according to an approximate flat plate boundary layer for the aircraft's flight conditions. For the ICE model and the flight conditions of interest ($Re = 1.9 \times 10^6/\mathrm{ft}, M_\infty = 0.3$), the prismatic grid parameters are listed in Table 5.

Hybrid Splitflow uses a two-equation turbulence model for accurate solution of turbulent viscous flow fields. The k-kl and k-l models developed at LMTAS are comparable in accuracy to the k-ϵ and k-ω turbulence models, but they do not require nearly as fine near-wall grid spacing as do those models [11, 12]. In addition, unique and consistent wall function boundary conditions have been developed for the k-kl and k-l turbulence models.

For this study, the k-kl model was used without the wall function boundary condition. The viscous sublayer and buffer regions of the turbulent boundary layer are within the prismatic grid. The model has been validated for both attached and separated turbulent flows. Unlike the k-ϵ model, no ad-hoc corrections are required at separation and reattachment points to obtain reasonable solutions. The k-kl model has been applied extensively to a wide variety of aerospace flows and has been shown to be robust and comparable in accuracy to other well calibrated two equation turbulence models [12, 13].

5 Metrics

In order to measure LMTAS aerodynamic capabilities with regards to its users in Advanced Design and Stability and Controls, metrics were produced in consultation with these groups at LMTAS. The metrics discussions focused on time, accuracy, and ease of use. The metrics presented in this report represent a combination of both what is *needed* and what is *wanted*. While these metrics are not necessarily met in the present study, such discussion to establish the desired parameters can be very useful in tool development.

5.1 Advanced Design Metrics

The Advanced Design group is mostly concerned with computing aerodynamic properties around multiple cruise and maneuver points. For their applications, one polar is not enough, but the number of polars depends on the configurations under study. Usually extra data points are necessary to determine the effect of deployed high-lift devices and to build a database of trim data.

An ordinary aerodynamic simulation schedule would require at least three trailing-edge flap settings, three tail deflections, and three leading-edge flap settings, resulting in approximately 27 polars. To be most useful, Advanced Design would like the results of a full matrix in 24 hours; ideally then CFD techniques are expected to be able to finish approximately one polar per hour. The Advanced Design group's current analysis techniques are not as fast at LMTAS, however—it takes about one week to do a complete analysis. The current analysis codes used run quickly, but each requires significant setup and post-processing time. However, if CFD were to reach the same turnaround time as the current method, it will become the preliminary aerodynamic design tool of choice.

Advanced Design's accuracy criteria focus on accurately computing the drag coefficient, C_D. Drag increments (ΔC_D) are sufficient for their needs, but the primary values of interest are lift, drag, and moment. For drag:

- $C_D \pm 5\%$ below polar break (cruise)
- $C_D \pm 10\%$ above polar break (maneuver)
- $C_{D_0} \pm 5\%$

Ease of use is also a large area of concern. To be useful, a tool has to be easy to use, or else the users will gravitate back to what they know. Ease is somewhat defined by how many training hours are required and the availability and clarity of any documentation. The number of parameters that need tweaking should not be very large; however, there should be enough parameters to cover all possible aspects of a problem being simulated. Ideally, one would have sets of parameters that would work well for a given class of problem, perhaps with an expert system to choose given simple input (perhaps α, wing sweep angle, t/c, and aspect ratio).

User interface is a significant part of ease of use. Standard Fortran-type inputs, such as namelists and formatted inputs, can cause long delays where the computer gives no meaningful error message and refuses to proceed—often over a simple typographical error in the input. Also, automatic grid generation is very sensitive to the quality of the input surface mesh, and some method is required to clean up the surface. Finally using *Splitflow*, "split cells" are often a problem. Split cells occur where the cell is cut into multiple disjoint volumes by the body. Refining the grid does not always solve the problem and may be more costly than allowable. To be useful where the geometry is changing rapidly (as in the early design cycle), geometric problems such as gaps, poor triangulations, or too-thin bodies must be fixed early in the process.

The LMTAS Advanced Design group's current methods are adequate, but they are still interested in improvements. Most of their methods are based on linear theory, so it is expected that any improvements will come through the proper accommodation for nonlinear aerodynamics. The required level of theoretical and geometric modeling, however, is not yet determined.

5.2 S&C Metrics

Stability and Controls (S&C) metrics are based on the conclusions reported in [14], with modifications provided by the LMTAS Stability and Controls group. Their key concern is to get reliable data from a combination of experimental databases, linear methods, and advanced CFD methods for potentially complex configurations. Their goals are to obtain methods that are simple and quick, but again accuracy is very important. In summary, force and moment coefficients are needed to the following accuracy:

- $C_L \pm 5 \sim 10\%$ if the flow is attached, $\pm 10 \sim 20\%$ if it is partly separated, and $\pm 20 \sim 30\%$ if it is fully separated.
- Pitch, roll, and yaw-moments $\pm 20\%$ of data range, within 2° of zeroes.

These requirements do not cover trim nor performance restrictions. S&C analysis assumes that once the aircraft is near the right configuration, the control system can appropriately counter any unanticipated force or response. Even the magnitudes of the forces and moments are not so important as the signs, i.e. the system needs to know which way to push, but it is assumed that the control system has sufficient force to accomplish the task. (While this is the assumption, it is critical to know that a given deflection in control surface will produce correct direction of force and moments—this could be a particular problem with phenomenon such as aileron reversal.)

5.3 Runtime

Since *Splitflow* was intended to be an automatic grid generator and flow solver, the setup time for *Splitflow* is minimal. Once the CAD surface cleanup is complete, one configuration setup usually works for all of the runs. The computations, however, took much longer than anticipated.

Reruns were often required, often to compensate for thin-wing based split cell problems on the ICE configuration. There are only two known ways to deal with split cells using *Splitflow*:

1. reduce `dxyzmin` allowing cells to be cut smaller than the body thickness, so each side is properly handled.
2. or zero `mxdelete` causing no grid coarsening with grid adaption, and *reducing* the chances of producing a split cell.

Both of these values are described in [15]. Decisions regarding their use fall to the user's discretion.

Boundary condition and turbulence models also caused some difficulty. In particular, when attempting to use a (less expensive) slip BC on the sting, the turbulence model would fail and crash the code. Finally, The *Omnigrid Splitflow* flow solver appears to be considerably less efficient than the older *Hybrid-Splitflow* code, and this greatly affected turnaround, as discussed in more detail in Section 6.9.

6 Results

Results for this analysis are presented according to the following list. Individual plots are included in Sections 6.1 and 6.2 for the MTVI and ICE configurations, respectively. For each data set, six plots are included, for the body-axis forces (F_x, F_y, and F_z) and body-axis moments (M_x, M_y, and M_z), in that order.

- MTVI, α-sweep
  - $\beta = 0°$
  - $\beta = 2°$
- Tailless Delta (ICE), α-sweep
  - $\beta = 0°$
  - $\beta = 5°$
  - $\beta = 10°$
  - $\beta = 20°$
- Tailless Delta (ICE), β-sweep

The coefficients of interest are:

- F_x, F_y, F_z force coefficients in the x-, y-, and z-directions (body axis) respectively.
- M_x, M_y, M_z moment coefficients about the x-, y-, and z-directions (body axis) respectively, also referred to as C_l, C_m, C_n and CLLB, CLM, CLNB.

The MTVI runs performed are listed in Table 1, while the ICE runs are listed in Tables 2, 3, and 4 for the α-sweeps, β-sweep, and viscous series respectively. The chosen test matrix for these cases covers a wide variety of angles of attack and sideslip for the two similar configurations, MTVI and ICE. While expanding the range of either variable (particularly sideslip for falling-leaf predictions) would be helpful, a lot has been learned regarding how to analyze cases such as this and where some of the potential pitfalls lie. As expected, the use of the Euler equations as a physical basis improved the prediction capability for nonlinear phenomenon. Although not reported here, as expected, nonlinear phenomenon related to viscous effects (vortex breakdown, separation and reattachment, etc.) were not predicted well.

The "acceptable prediction ranges" (grey areas) on the moment coefficient plots in Sections 6.1 and 6.2 are based on the S&C criteria discussed in Section 5.2. Since the focus is on moment coefficients at nonzero β, only those are specifically shown on the included plots. Here, a tighter tolerance of only $\pm 10\%$ is used to better demonstrate areas of success and desired improvement—$\pm 20\%$ of the data range is 40% of the data range, as specified by the S&C criteria, or nearly *half* the plotted area. These regions are hand-drawn on underlays for the plots using *Tecplot* [16], and they represent an approximate (not numeric) region of acceptability. The computed results also contain "error bars," which show the fluctuation in force or moment coefficient over (approximately) the last 100 iterations.

The linear theory results are produced by the *HASC* code [17]. *HASC* uses linear theory models modified through experience at analyzing high-performance aircraft.

6.1 MTVI

The MTVI results did not turn out as well as expected. While some of the nonlinear breaks were captured near the correct α, the magnitudes were often significantly different than the wind-tunnel data. Part of the problem is the wide range of angle of attack, $0 < \alpha < 45°$. At large α, much of the flow is separated into complex vortical flows, and in some instances vortex breakdown causes unsteady flows that are difficult to simulate even with Navier-Stokes methods.

6.1.1 MTVI Results, $\beta = 0°$

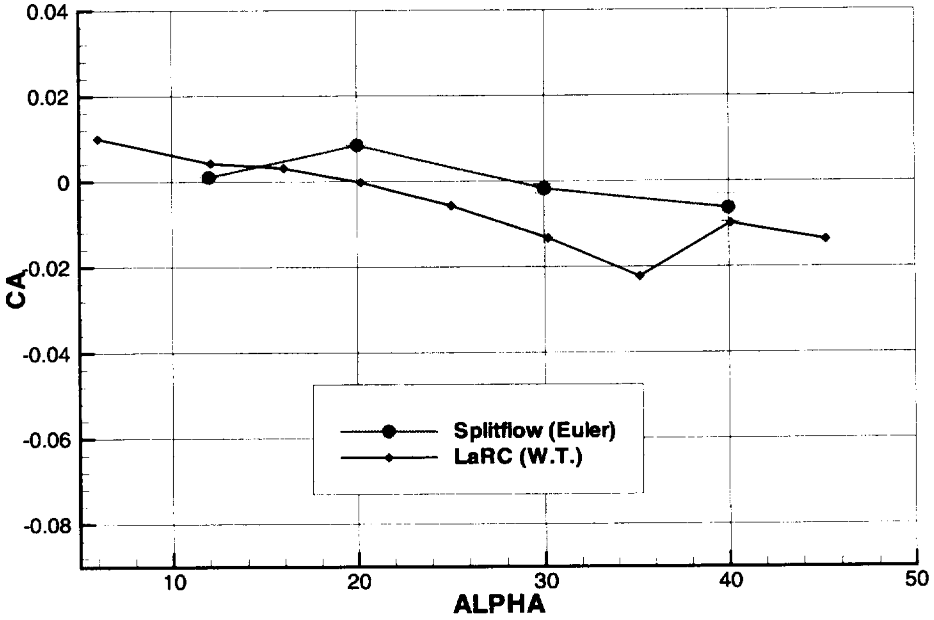

MTVI, $\beta = 0°$, F_x

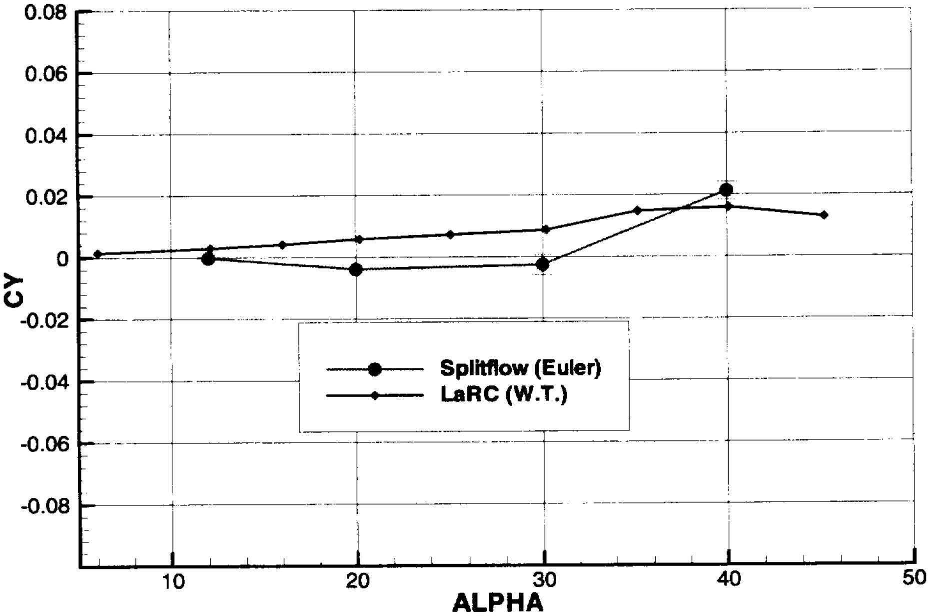

MTVI, $\beta = 0°$, F_y

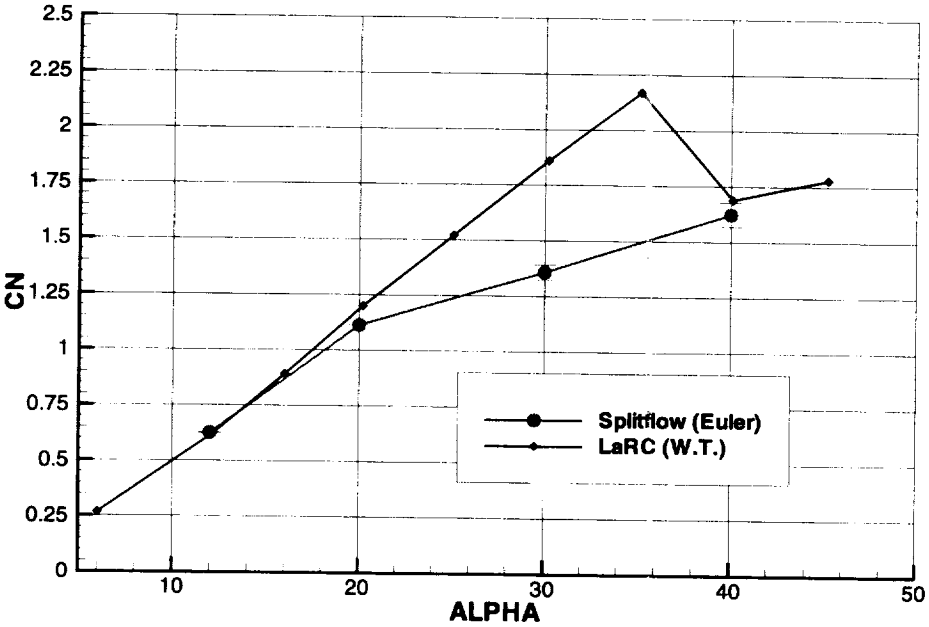

MTVI, $\beta = 0°$, F_z

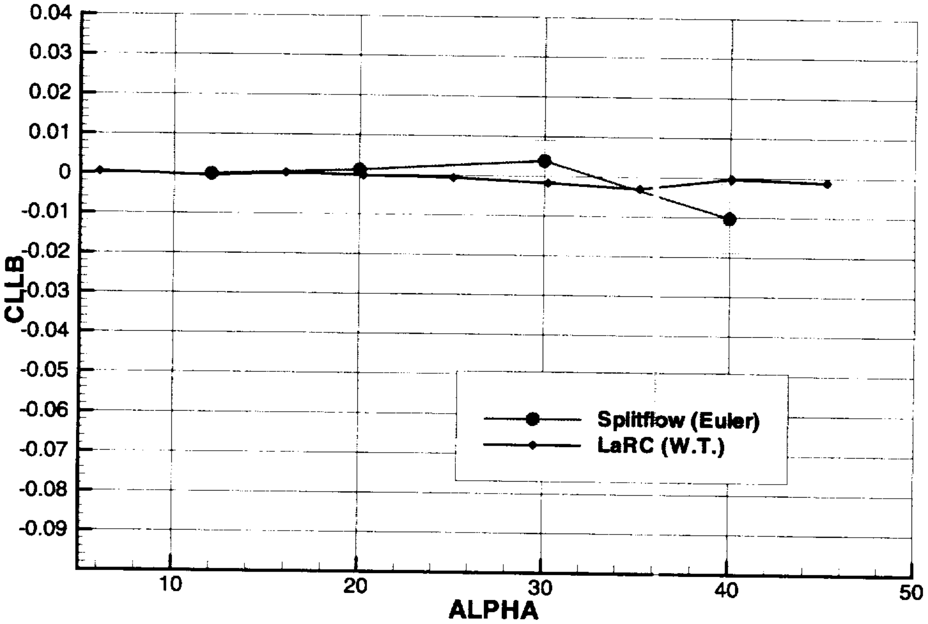

MTVI, $\beta = 0°$, M_x

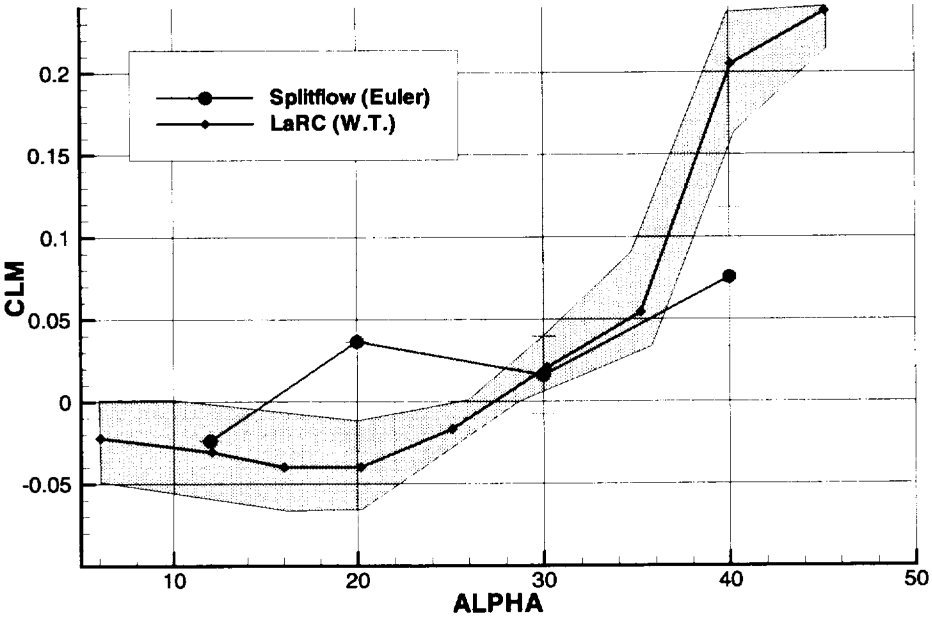

MTVI, $\beta = 0^\circ$, M_y

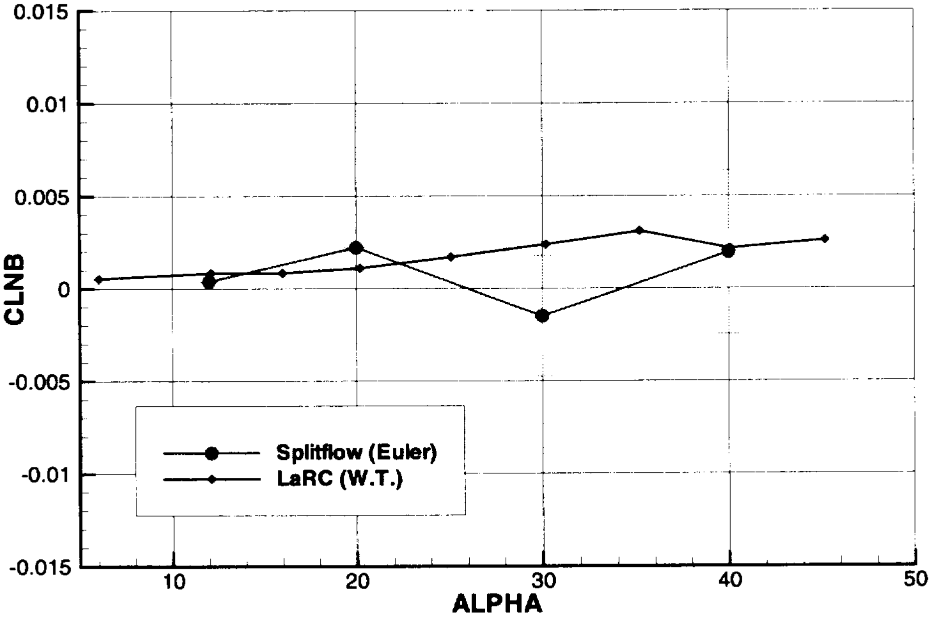

MTVI, $\beta = 0^\circ$, M_z

6.1.2 MTVI Results, $\beta = 2°$

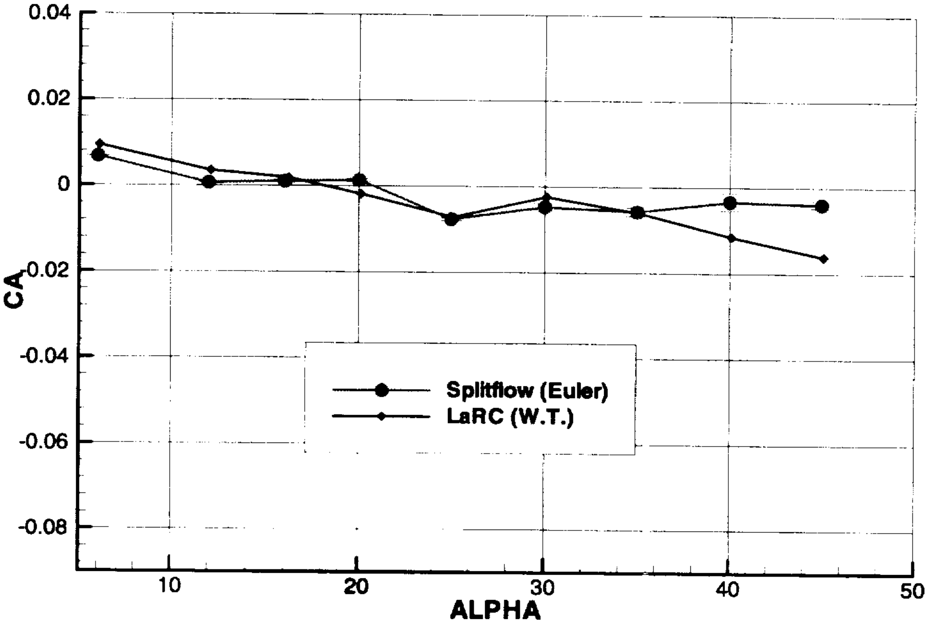

MTVI, $\beta = 2°$, F_x

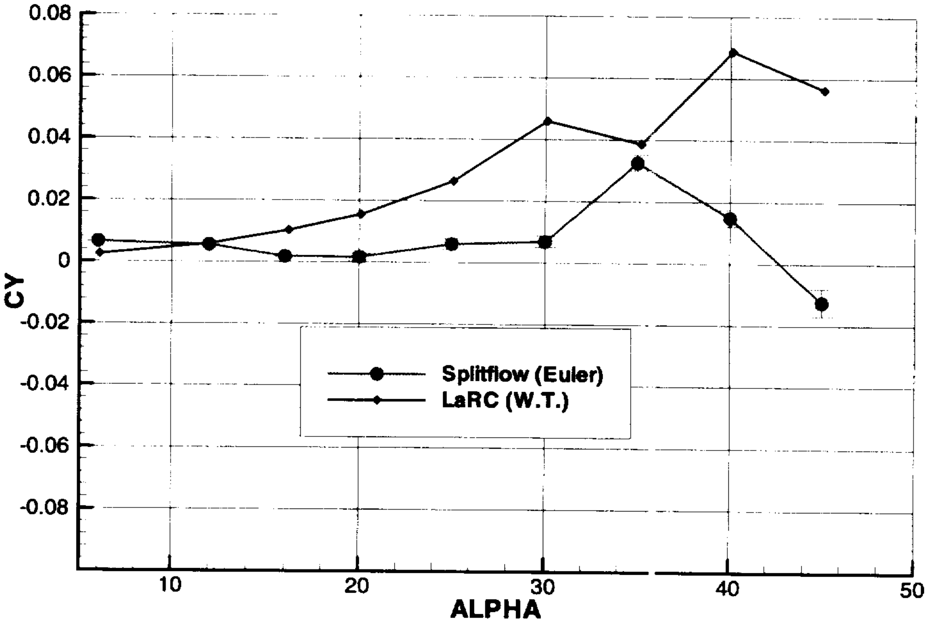

MTVI, $\beta = 2°$, F_y

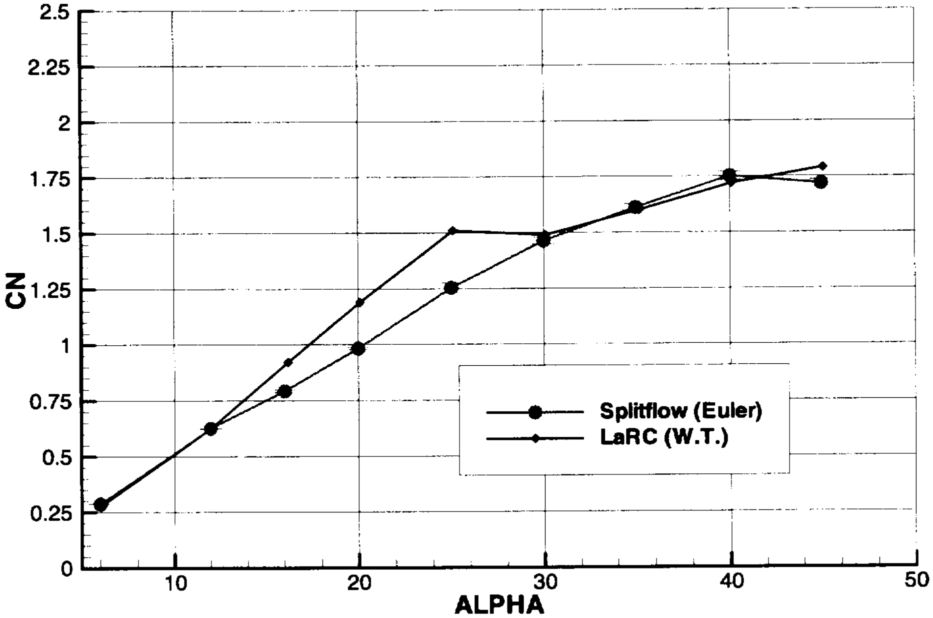

MTVI, $\beta = 2°$, F_z

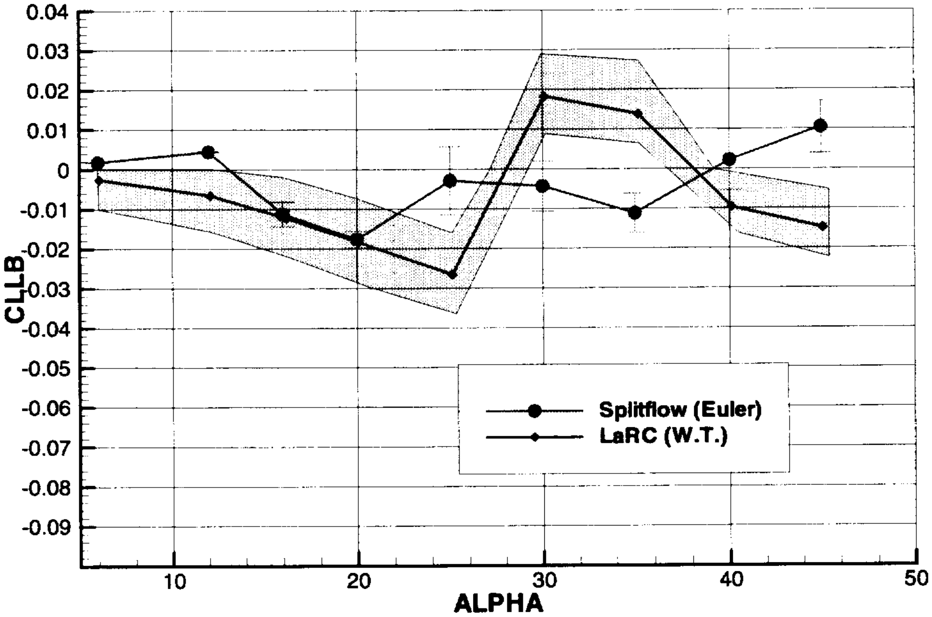

MTVI, $\beta = 2°$, M_x

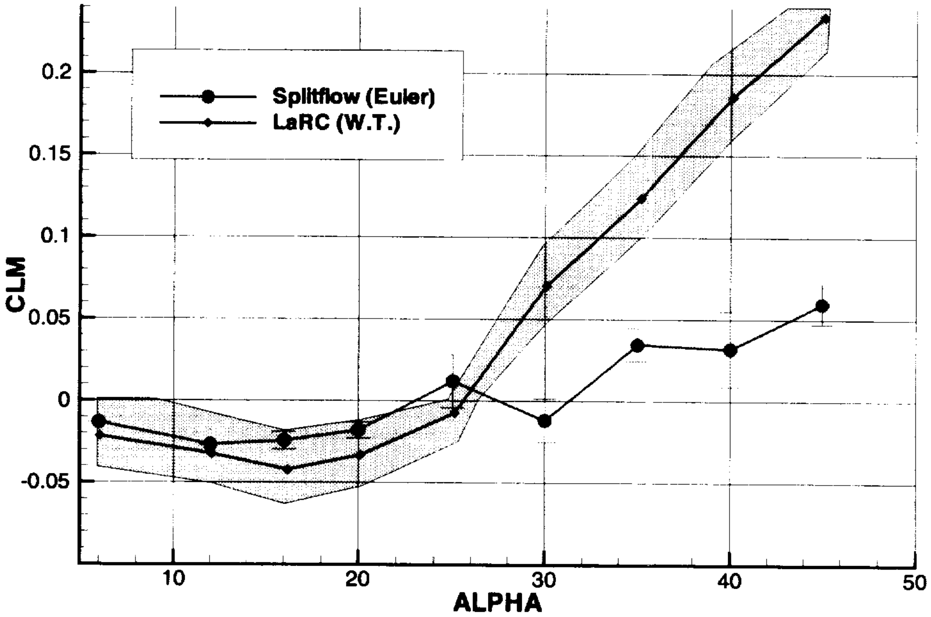

MTVI, $\beta = 2°$, M_y

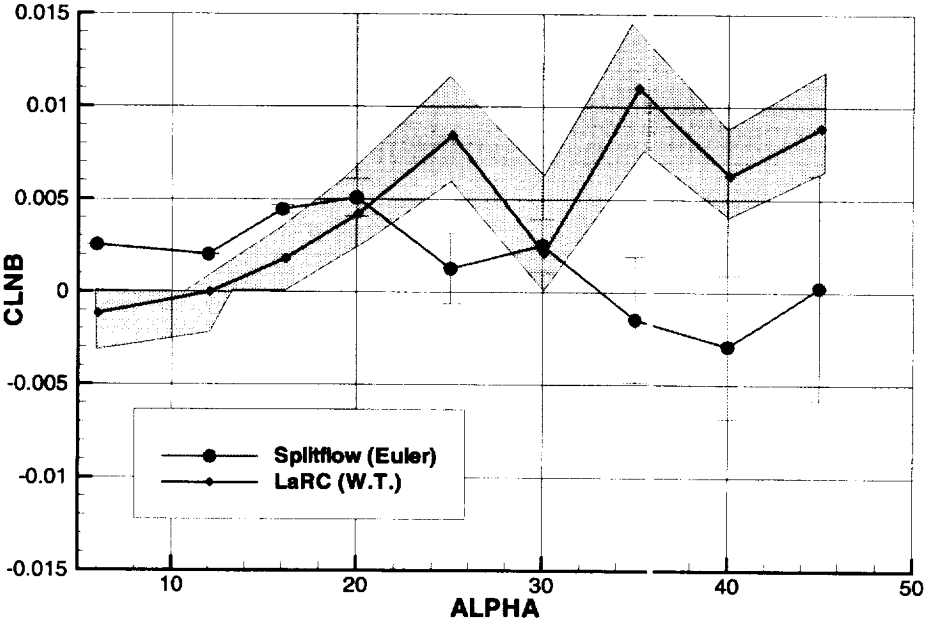

MTVI, $\beta = 2°$, M_z

6.2 ICE

The ICE results turned out much better, but they are still far from ideal. In some cases, the method was inadequate to predict certain nonlinearities present in the wind tunnel data, which could be attributed to the inherent limitations of the the Euler equations. The Navier Stokes solutions were somewhat better. Perhaps a thicker prismatic grid, or a smoother transition from the prismatic grid to the Cartesian grid, would have improved them.

6.2.1 Tailless Delta (ICE) Results: $\beta = 0°$

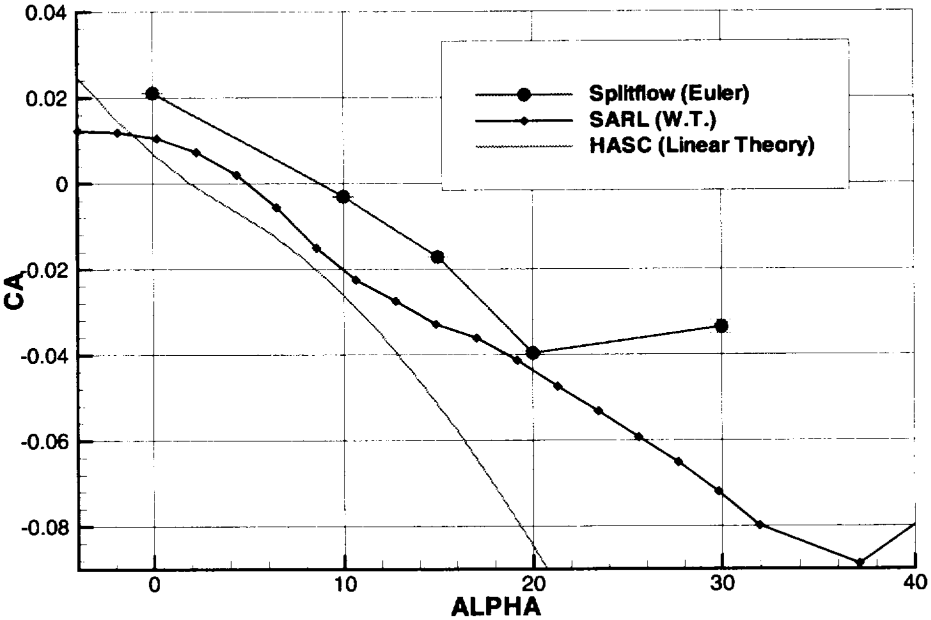

ICE, $\beta = 0°$, F_x

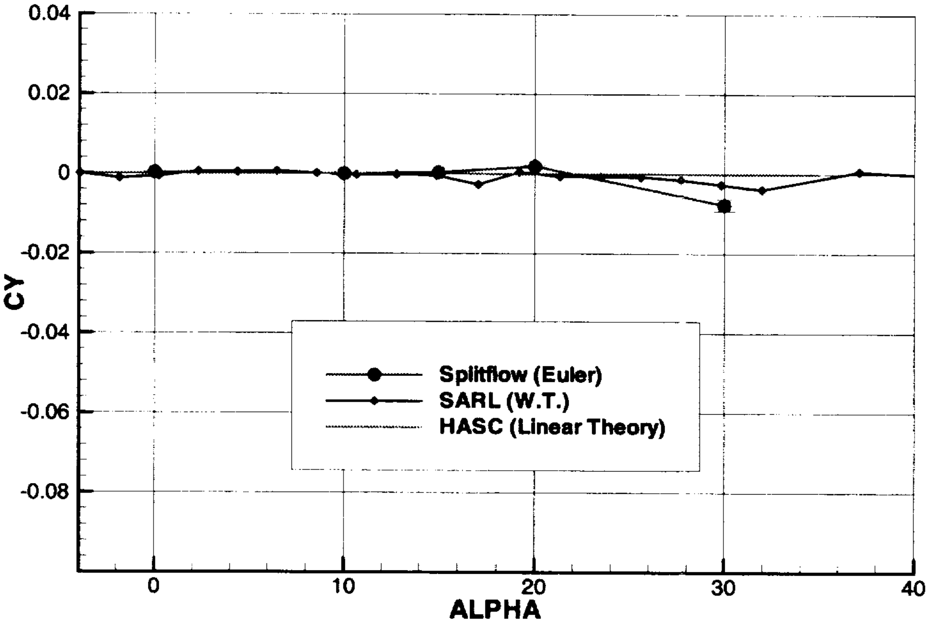

ICE, $\beta = 0^\circ$, F_y

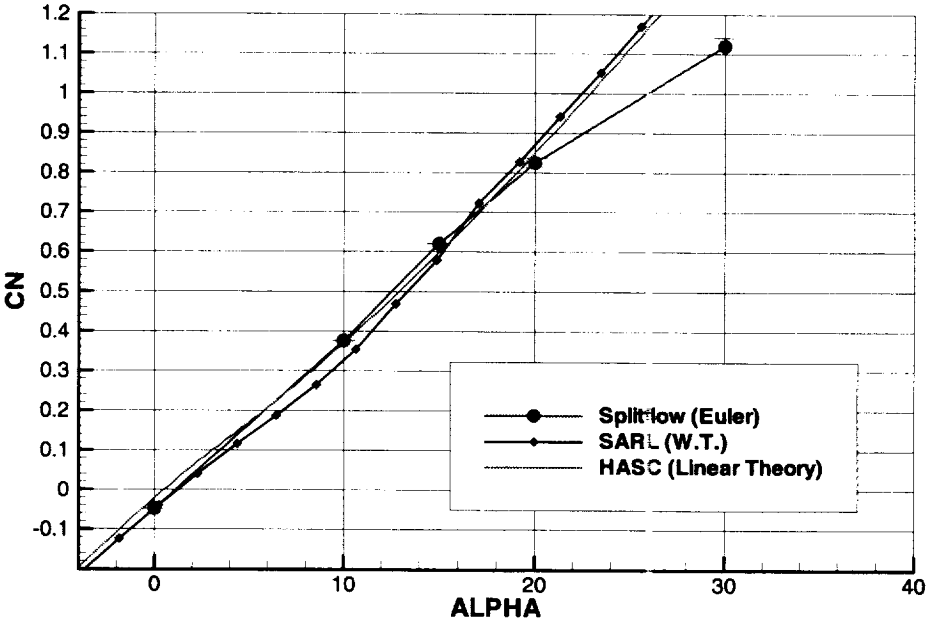

ICE, $\beta = 0^\circ$, F_z

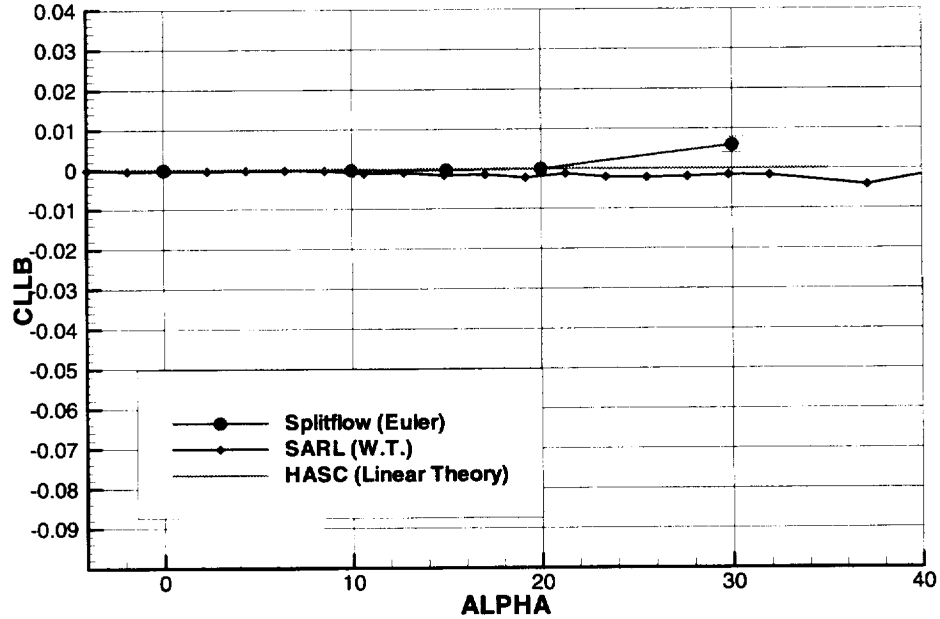

ICE, $\beta = 0°$, M_x

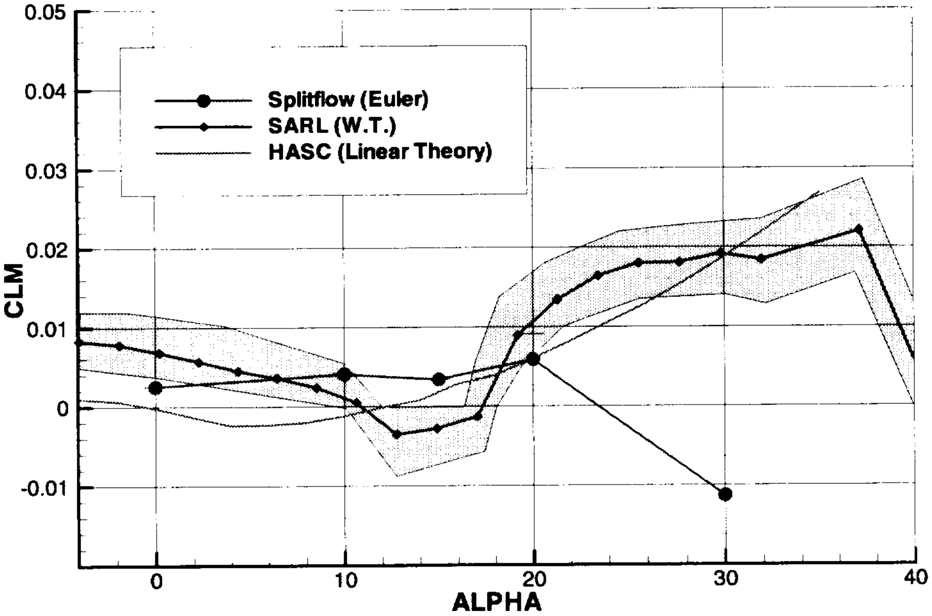

ICE, $\beta = 0°$, M_y

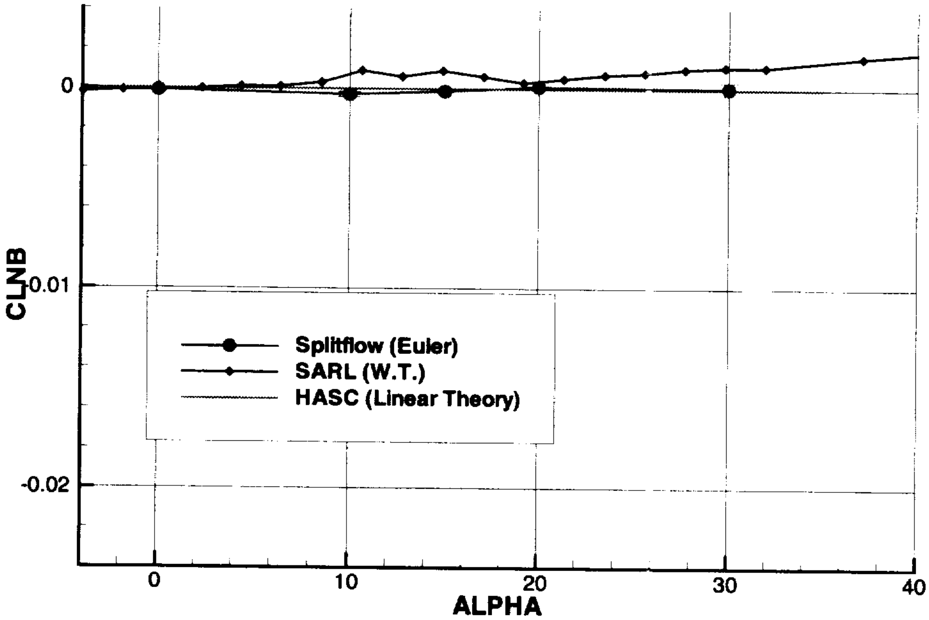

ICE, $\beta = 0°$, M_z

6.2.2 Tailless Delta (ICE) Results: $\beta = 5°$

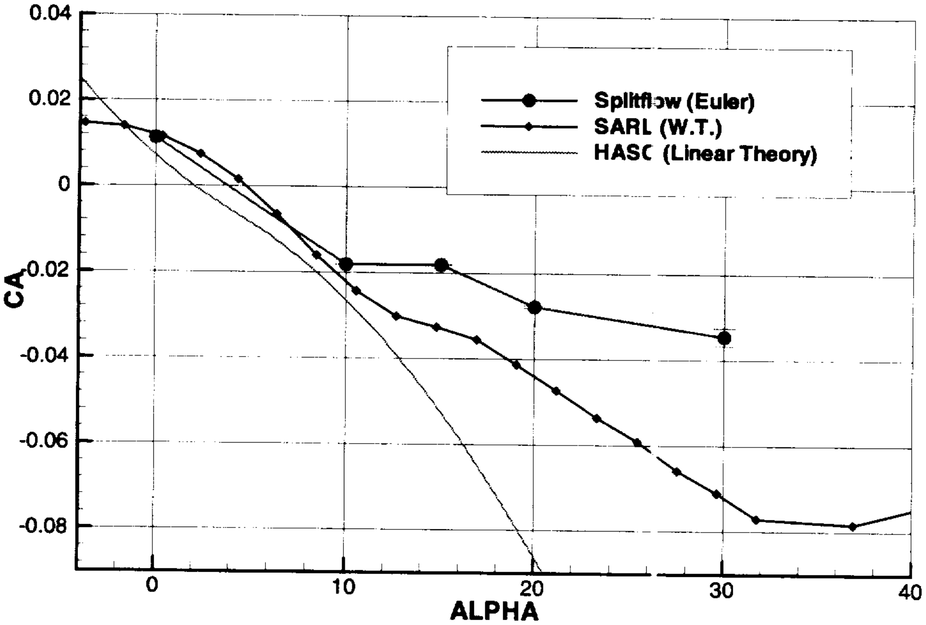

ICE, $\beta = 5°$, F_x

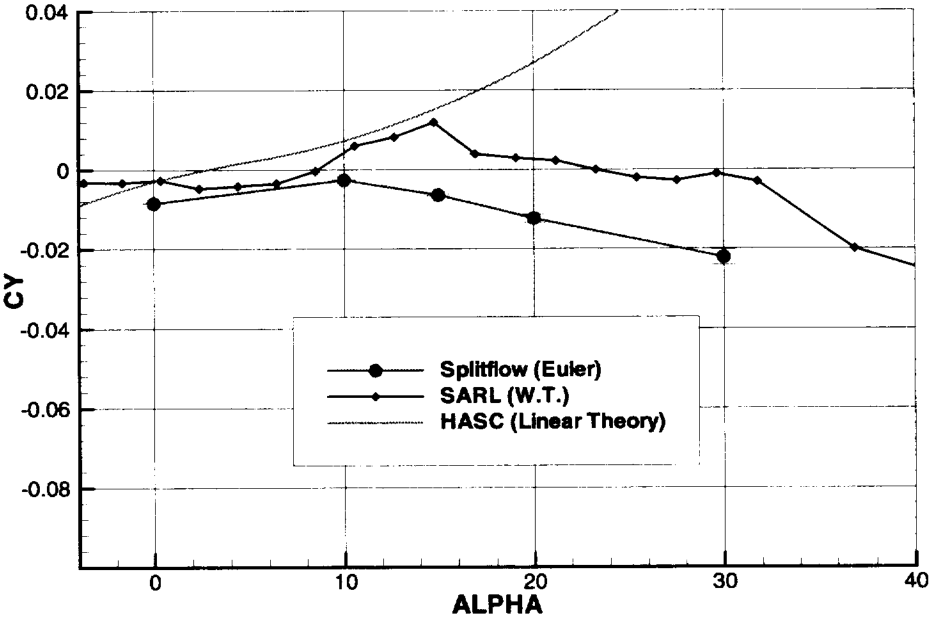

ICE, $\beta = 5°$, F_y

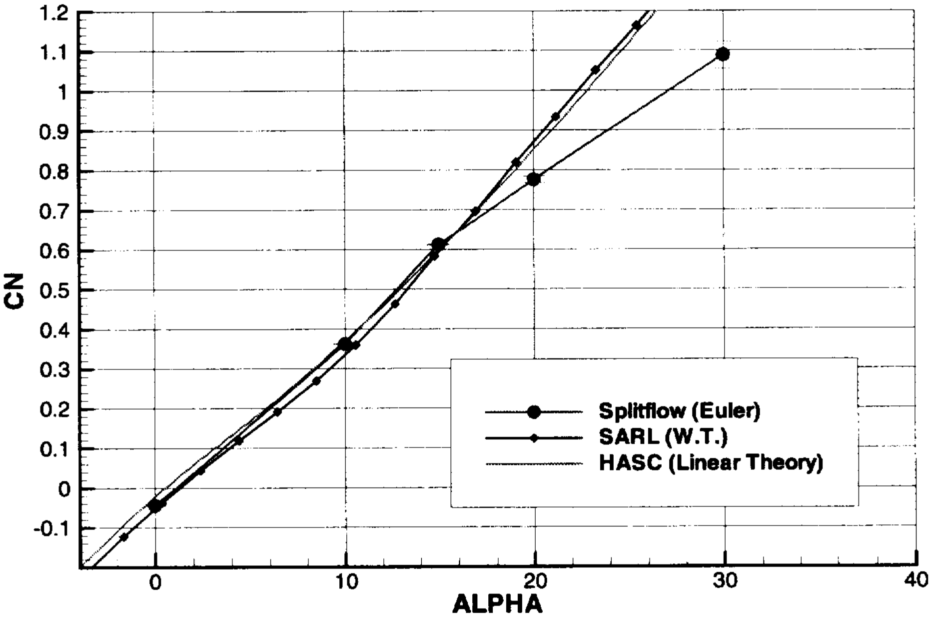

ICE, $\beta = 5°$, F_z

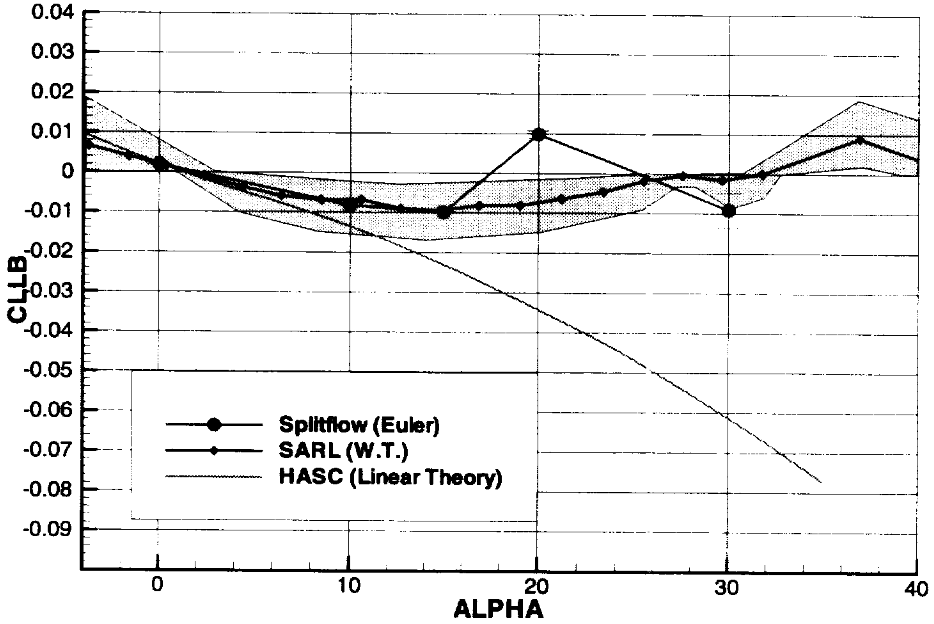

ICE, $\beta = 5°$, M_x

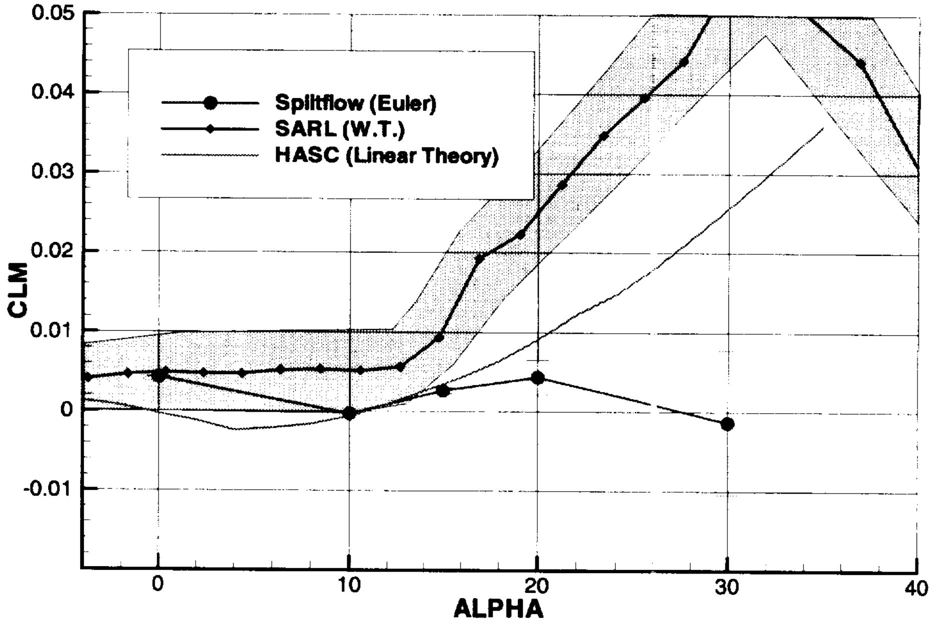

ICE, $\beta = 5°$, M_y

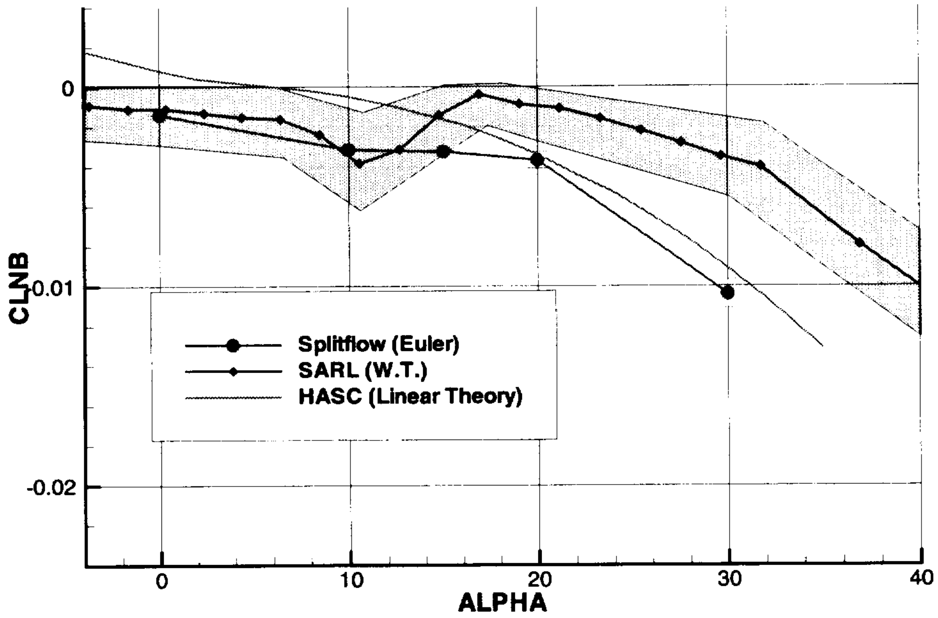

ICE, $\beta = 5^\circ$, M_z

6.2.3 Tailless Delta (ICE) Results: $\beta = 10^\circ$

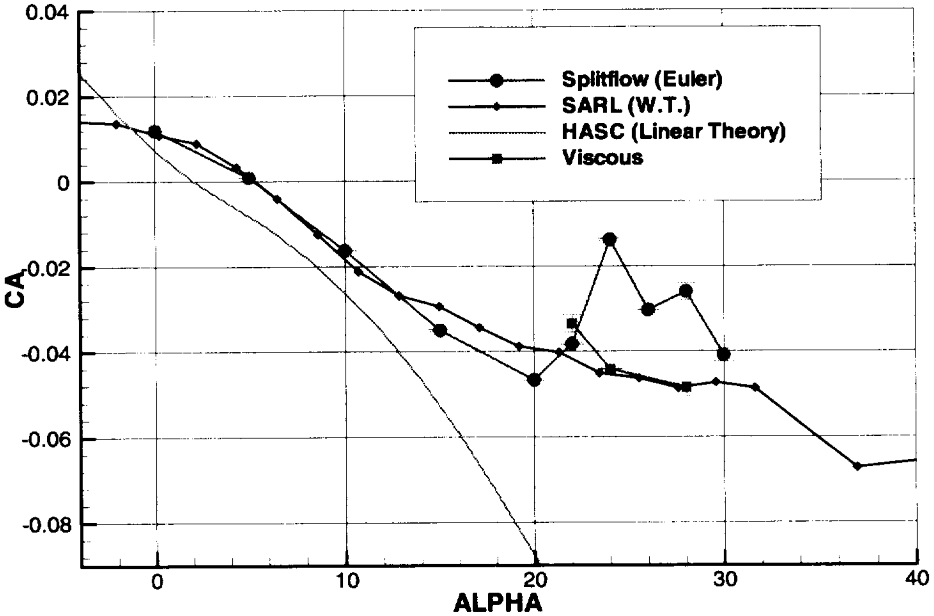

ICE, $\beta = 10^\circ$, F_x

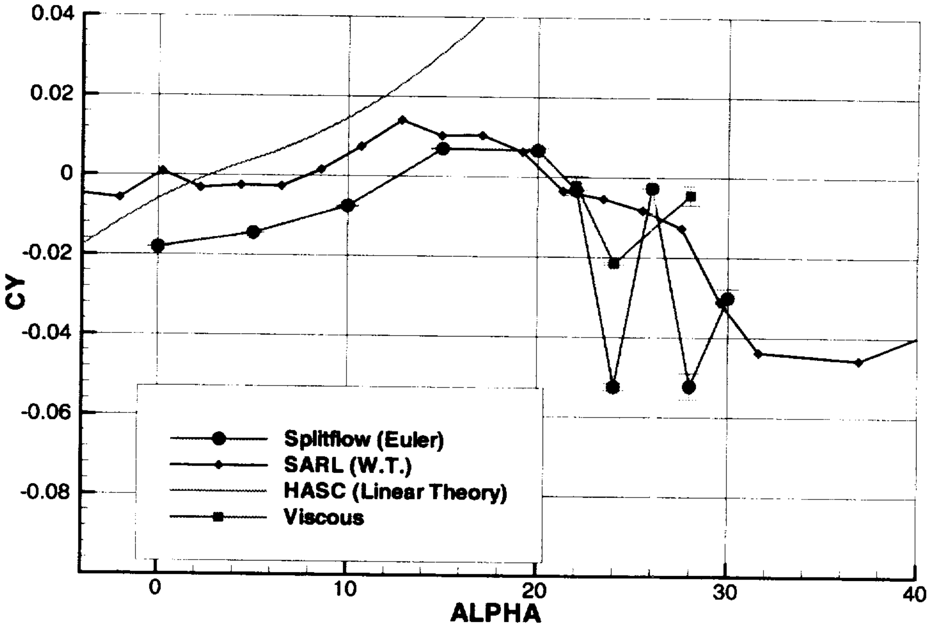

ICE, $\beta = 10°$, F_y

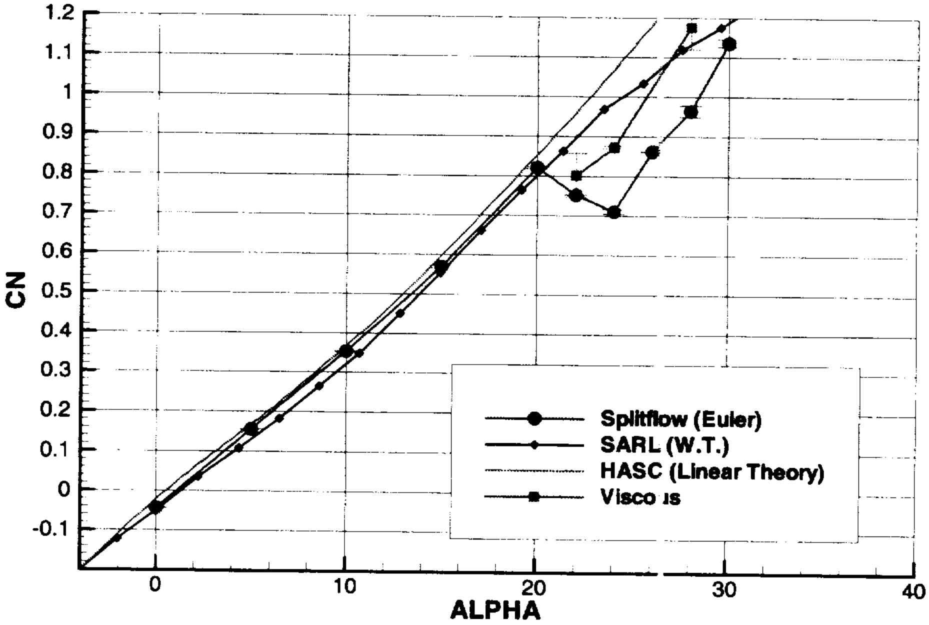

ICE, $\beta = 10°$, F_z

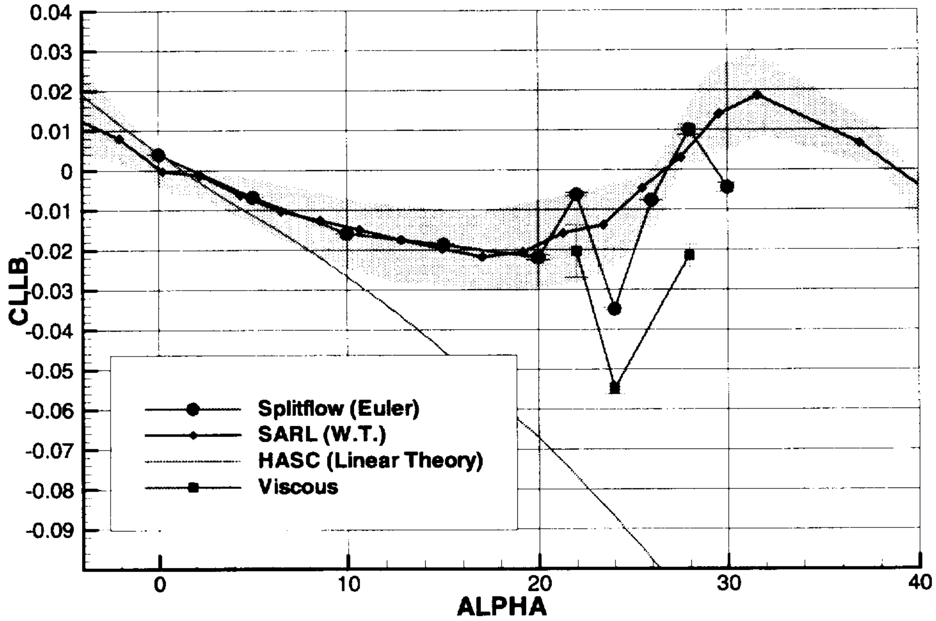

ICE, $\beta = 10^\circ$, M_x

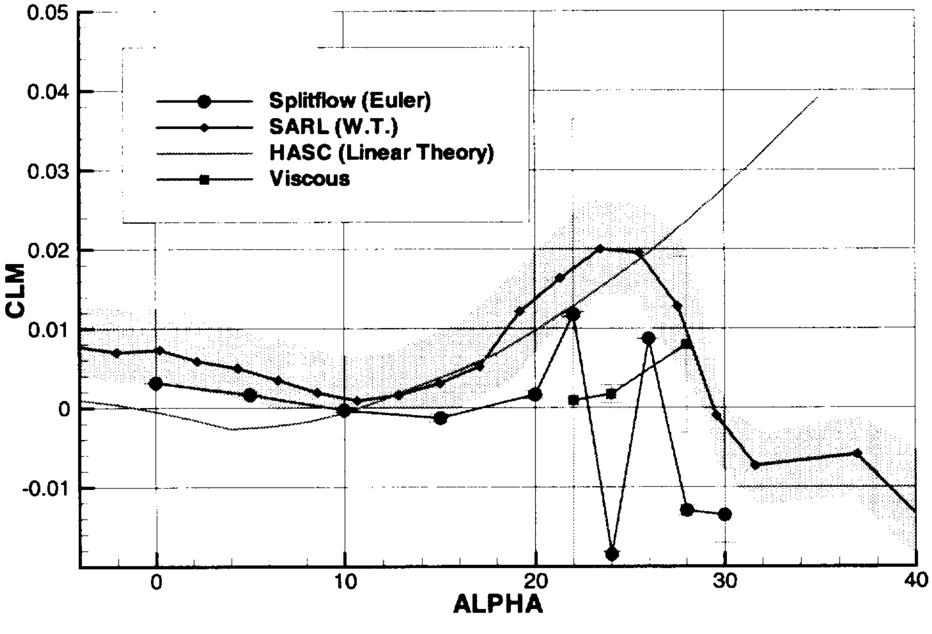

ICE, $\beta = 10^\circ$, M_y

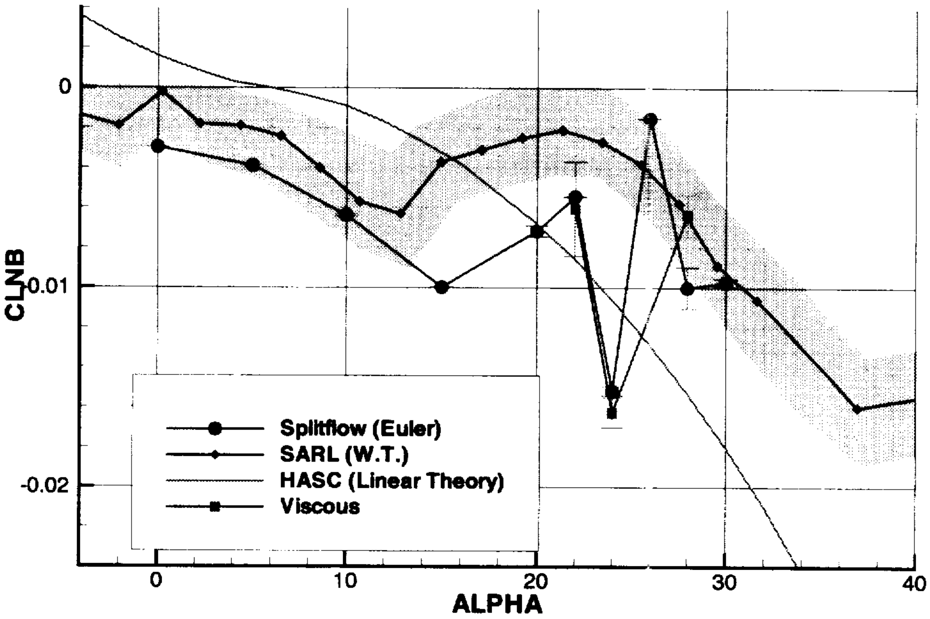

ICE, $\beta = 10°$, M_z

6.2.4 Tailless Delta (ICE) Results: $\beta = 20°$

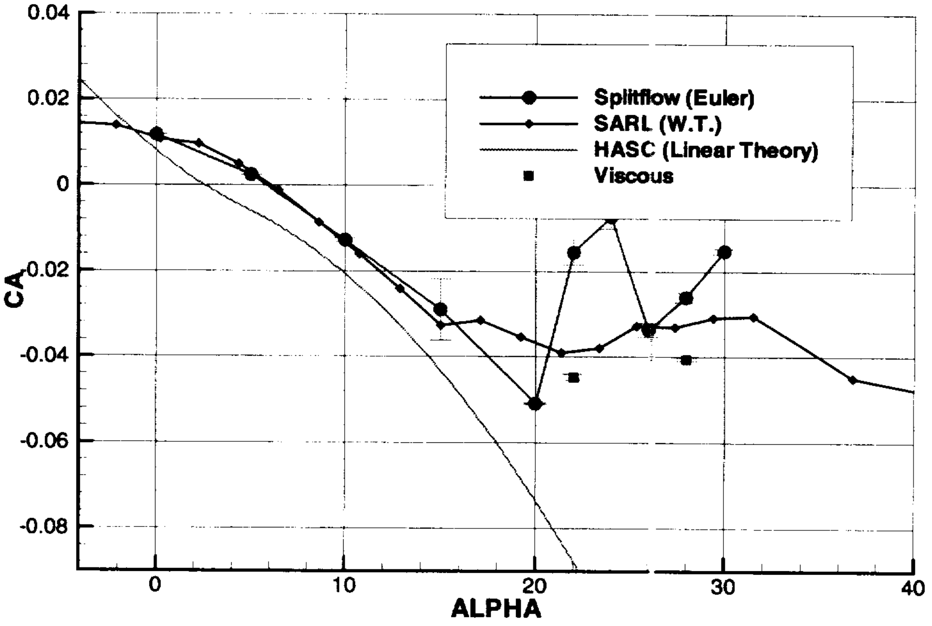

ICE, $\beta = 20°$, F_x

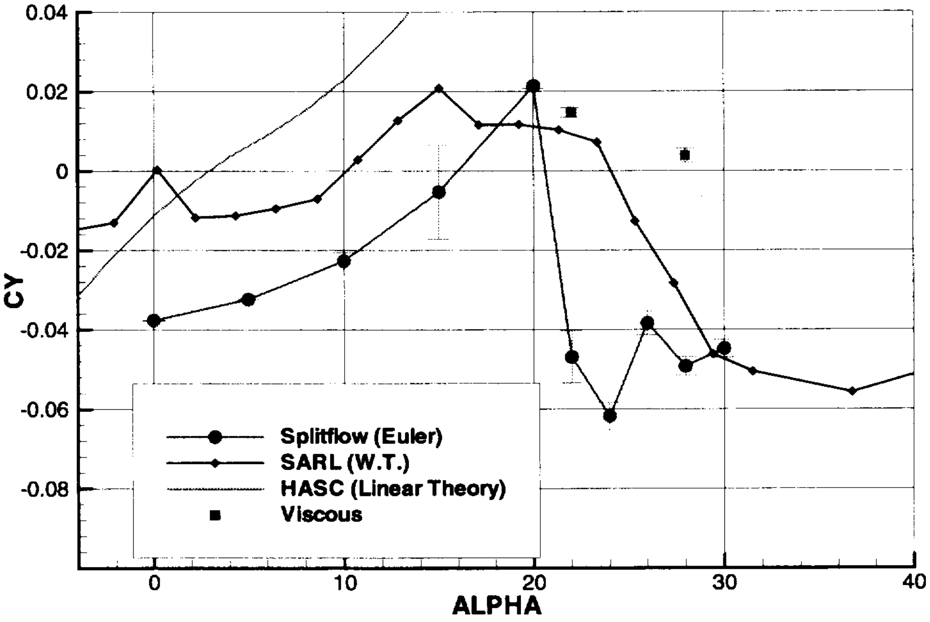

ICE, $\beta = 20°$, F_y

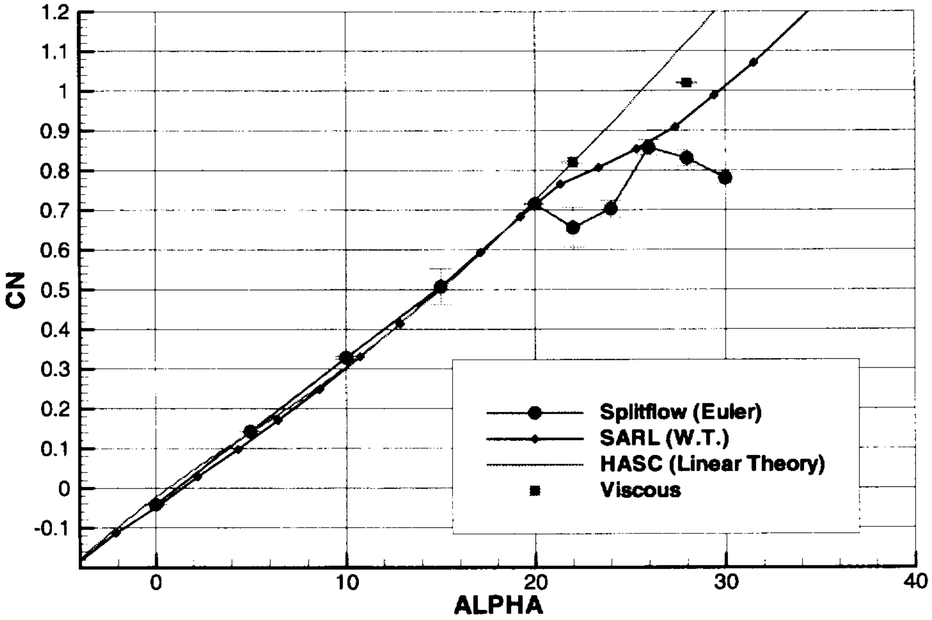

ICE, $\beta = 20°$, F_z

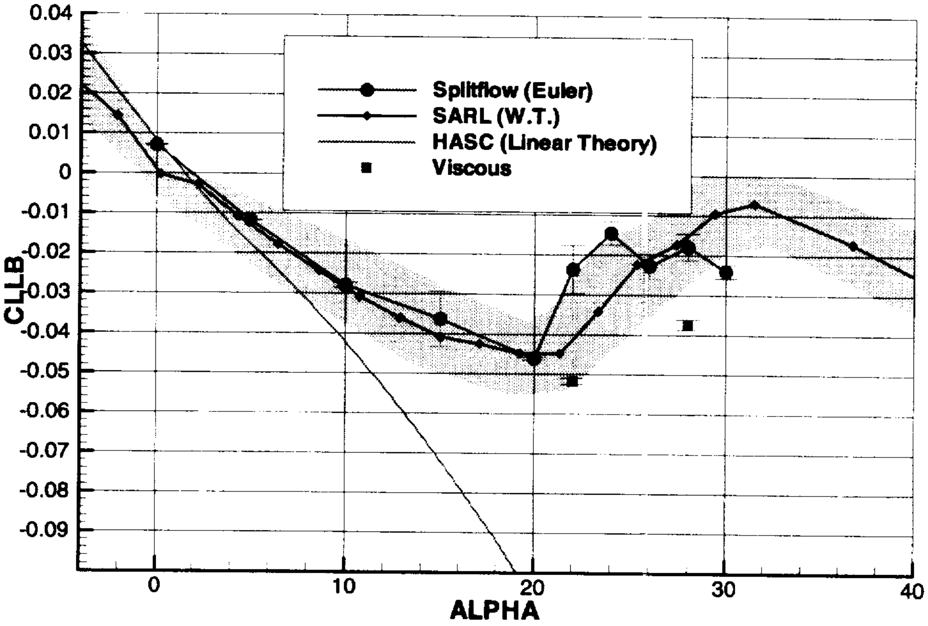

ICE, $\beta = 20°$, M_x

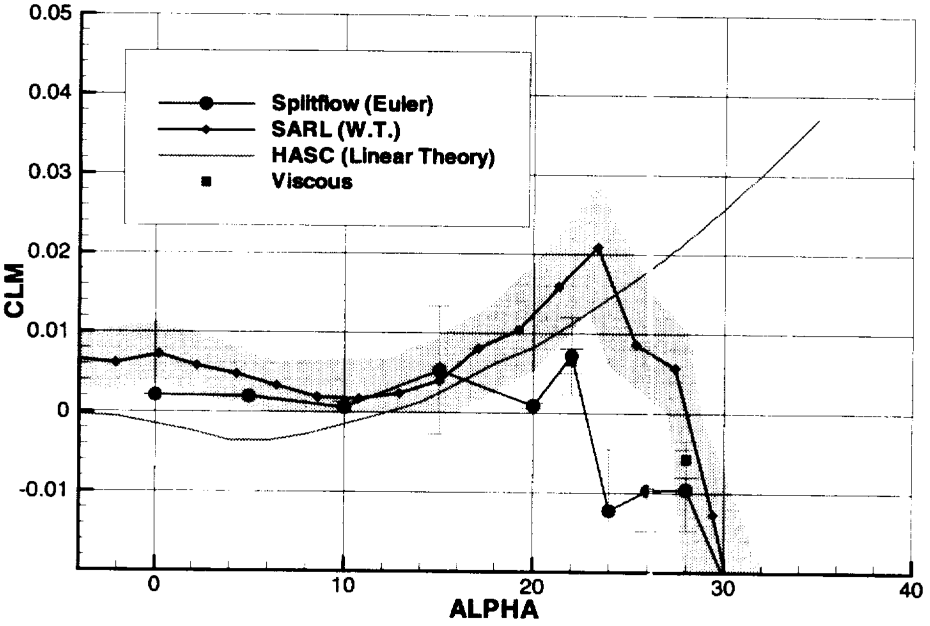

ICE, $\beta = 20°$, M_y

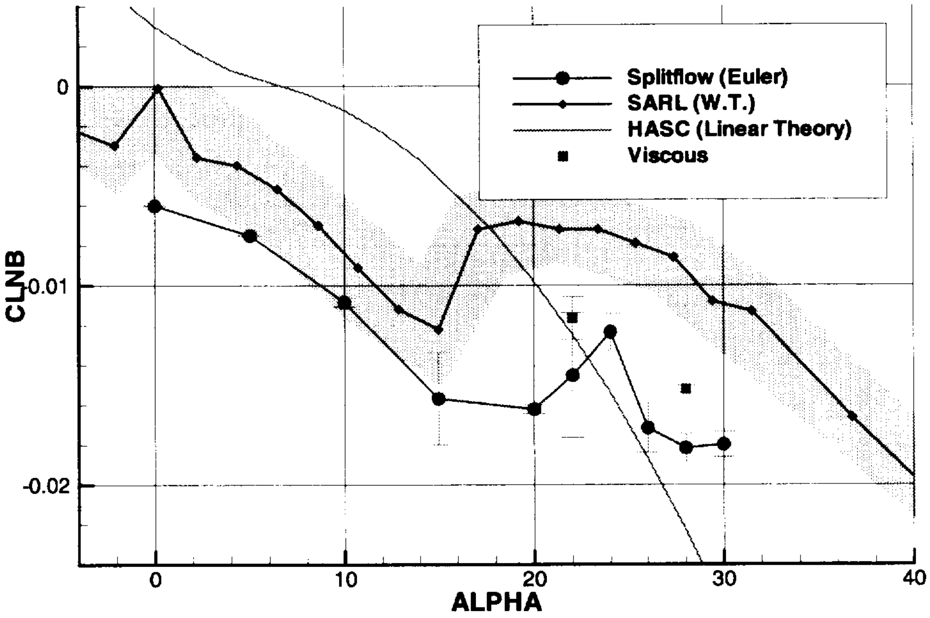

ICE, $\beta = 20°$, M_z

6.2.5 Tailless Delta (ICE) Results, β-sweep, $\alpha = 20°$

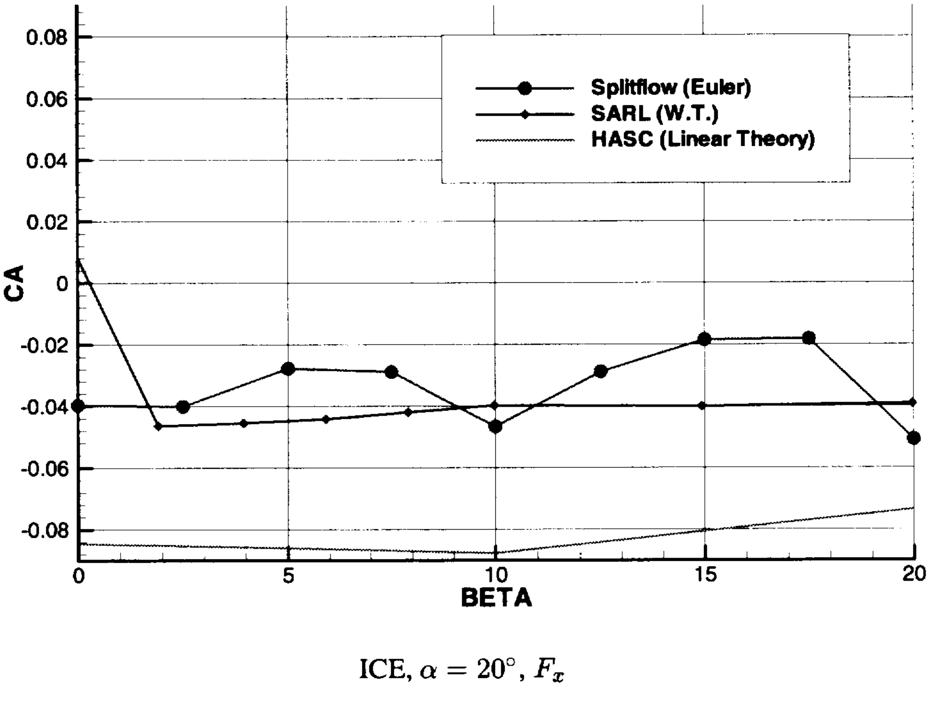

ICE, $\alpha = 20°$, F_x

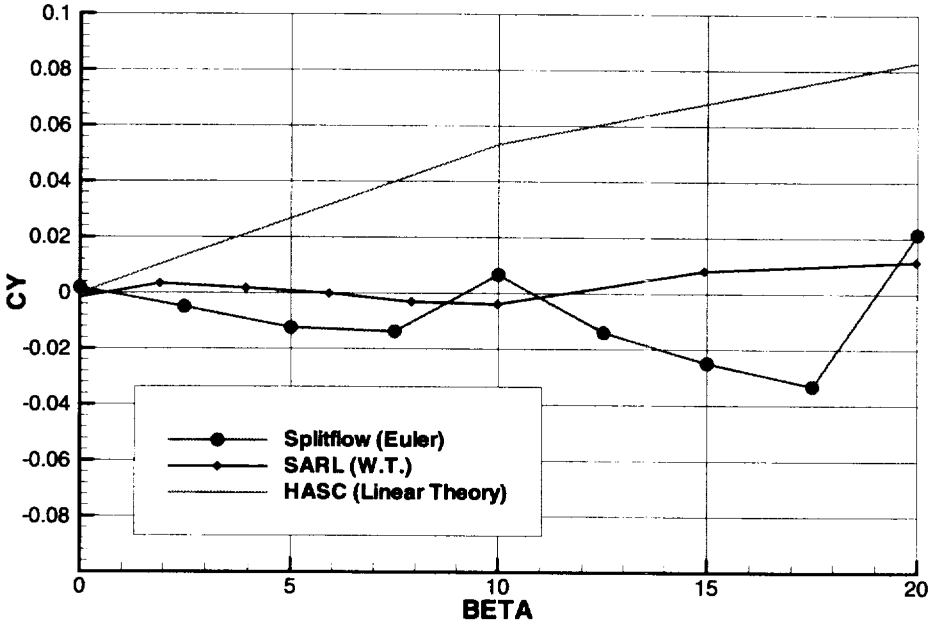

ICE, $\alpha = 20°$, F_y

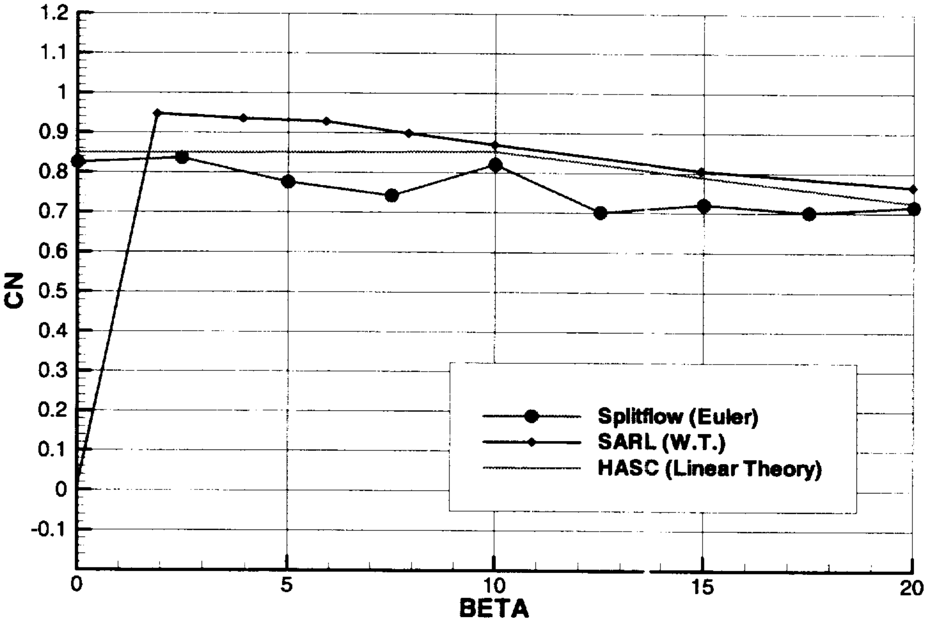

ICE, $\alpha = 20°$, F_z

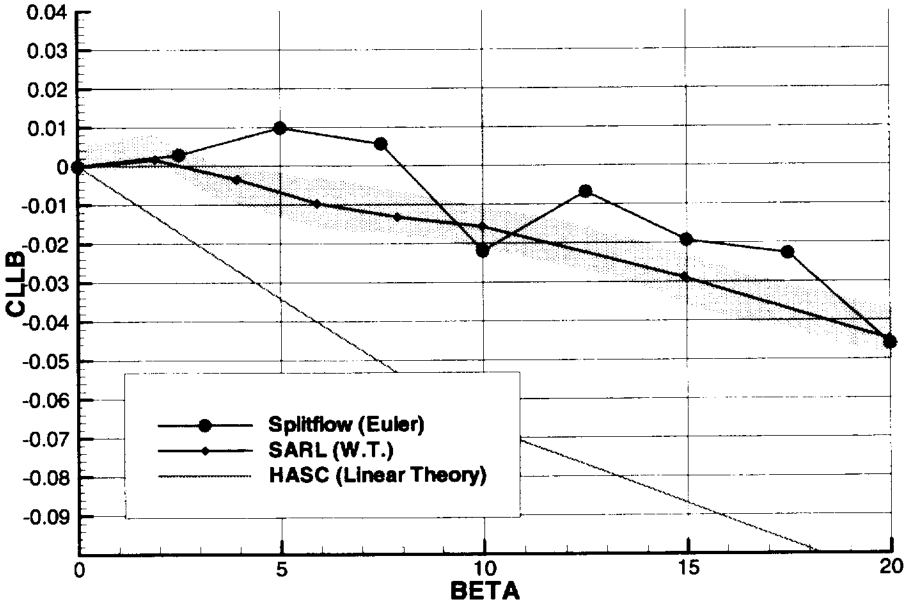

ICE, $\alpha = 20°$, M_x

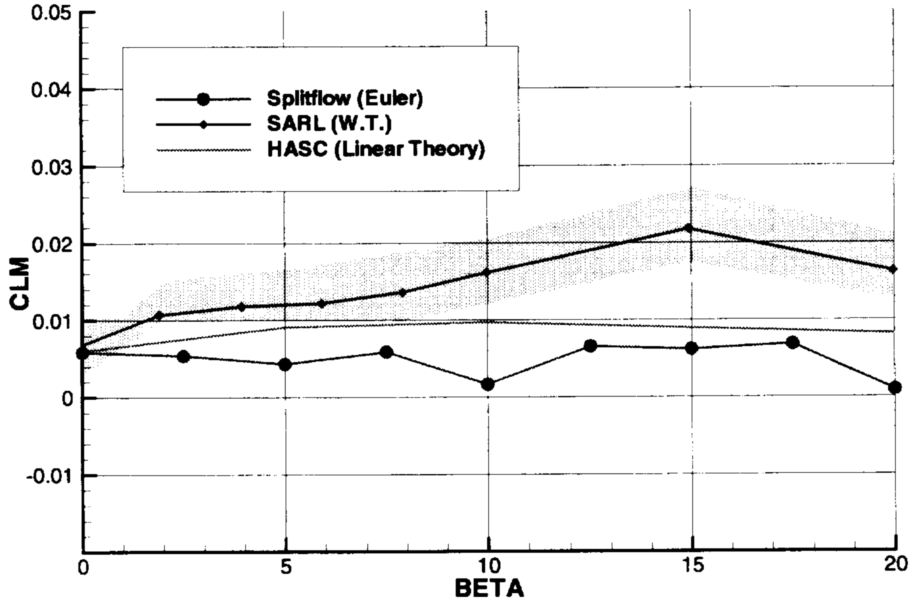

ICE, $\alpha = 20°$, M_y

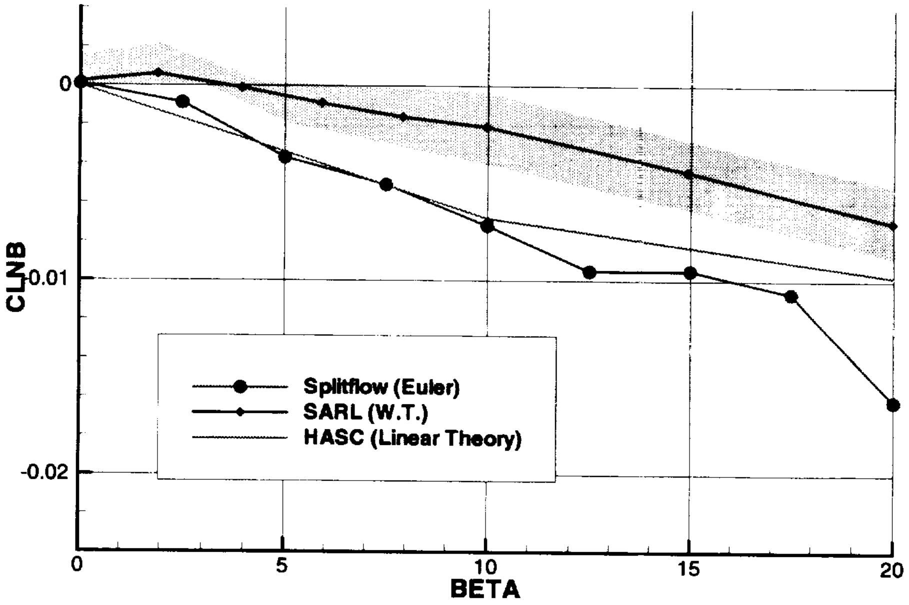

ICE, $\alpha = 20°$, M_z

6.3 Highlights

The numerical results for rolling and yawing moments were particularly impressive at low α ($\alpha < 24°$). Since the rolling and yawing moments are critical for the analysis of the falling-leaf condition, the fact that these parameters turned out well makes this technique very useful for its prediction.

The results for pitching moment appears particularly poor at $24° \leq \alpha \leq 30°$. Vortex breakdown and other viscous and unsteady effects are suspected to have contributed to this poor prediction. Also, even with 700,000 cells in the grid, the vortex cores were not well resolved.

The effect of grid resolution on solution accuracy was investigated and shown to yield little improvement, as discussed in Section 6.8. Regrettably, the extra work yielded little or no improvement. To check the numerical stability of the poor results at $\alpha = 24°$, the solution from $\alpha = 22°, \beta = 10°$ was restarted with conditions appropriate for $\alpha = 24°$. The result was that the pitching moment stayed approximately between the values at $\alpha = 22°$ and $\alpha = 26°$ for approximately 2,000 iterations before tumbling down closer to the values found starting from a uniform state. What originally appeared to be a hysteresis eventually broke down—this was originally believed to be a result of the adapting grid, but further tests on a fixed grid showed the same results. One important postscript is that these are not truly "grid converged" solutions in that respect, as they are grid dependent and true grid convergence studies are intended to eliminate that aspect of the computational problem.

6.4 Improvements

Originally, it was expected that new techniques that produced nice polars overnight on a workstation would be useful for the configurations presented here. These new techniques rely on extremely coarse volume grids ($\sim$ 100,000 cells) and overresolved surface grids (100,000 $\sim$ 300,000 triangles). These techniques have turned out surprisingly good results for transonic and supersonic wing/body configurations. However, both of the configurations in this present effort are vortex dominated at the flow speeds and angles used here, and the vortices require a large number of cells off the surface. Typically, convergence is delayed at the low speeds.

Figures 3(a) and 3(b) show a comparison of these results. "Original" refers to the first pass at solution of these problems, which involves running *Splitflow* on extremely coarse (approximately 100,000 cell) grids requiring only a few hours per case on a workstation. As shown in Figures 3(a) and 3(b) the coarse grid techniques produced unusably poor data, while the techniques described here did a reasonably good job of capturing the current nonlinear trends seen in the experimental data.

Some of the nonlinearities displayed in the CFD results with increasing α may be due to the complex vortical flows for these configurations. Disagreements have been found in results from different wind tunnels for the ICE configuration. Results from a different wind tunnel test show nonlinearities not apparent in the SARL tests.

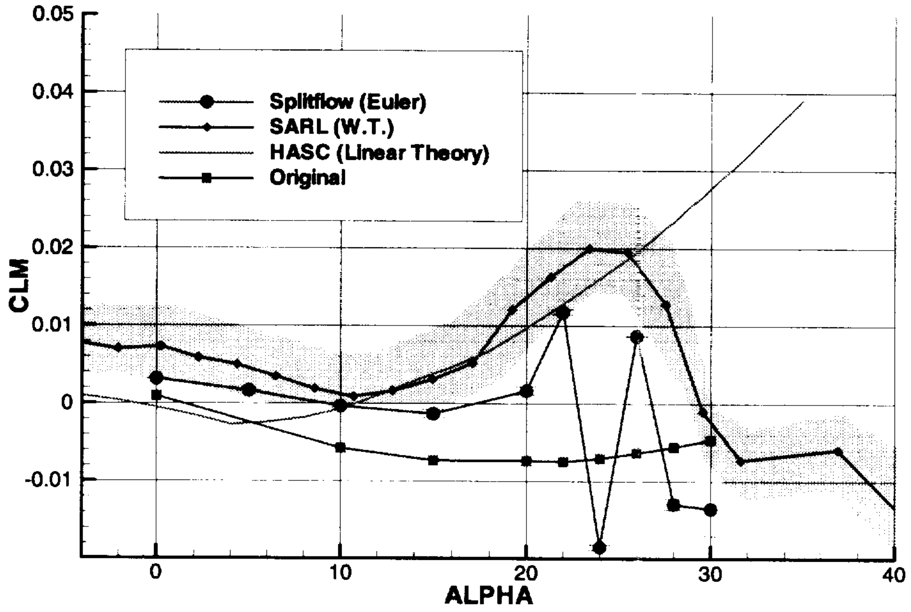

(a) $\beta = 10^\circ$

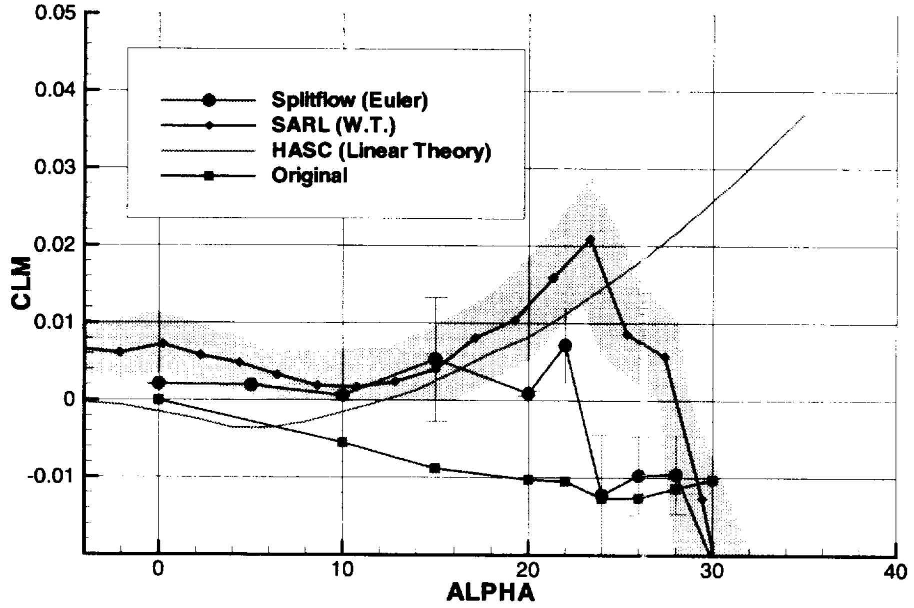

(b) $\beta = 20^\circ$

Figure 3: Improved M_y results for the ICE configuration

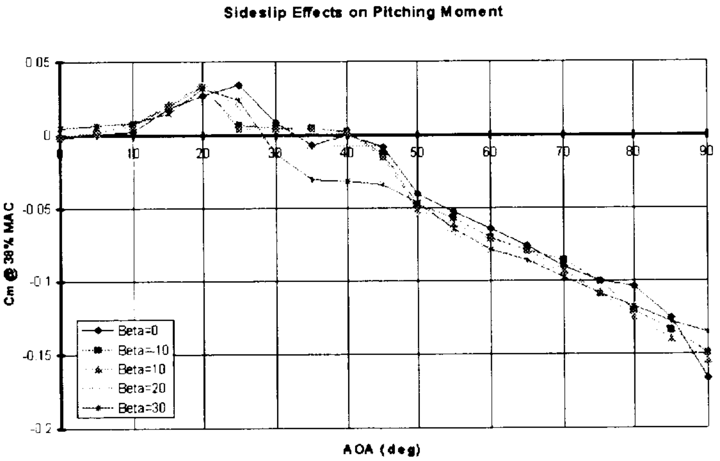

Figure 4: ICE model pitch moment rotary balance test data

Figure 4 shows pitch moment coefficient (M_y) test data for the ICE model from a rotary balance test in 1996 at the Bhirle Applied Research 10-foot vertical wind tunnel in Neuberg, Germany [18]. The test used a 1/13th scale model with dynamic and static data collection. Comparing Figures 3(b) and 4 for $\beta = 20°$, two important issues are the location of the curve crossing the axis and both the Bhirle measurements and the *Splitflow* computational results show a "leveling off" near 24° around zero M_y, before the value drops negative. These differences lead to a conclusion that there is some fundamental difference between the SARL wind tunnel tests and the inviscid simulations. Since the Bhirle data is taken at "low" Reynolds number, and the SARL data is at "high" Reynolds number, and inviscid simulations with *Splitflow* imply "low-but-not-controlled" viscosity (hence "high" Reynolds number), it is expected that some Reynolds number effect is appearing in this comparison.

6.5 Solution Adaption

Solution-based grid adaption was relied upon in *Splitflow* to yield highly-resolved solutions with a minimum number of cells and without expert setup. *Splitflow* can refine on many functions, but how does one decide what is important? Traditionally at LMTAS, helicity ($\vec{v} \cdot \vec{\omega}$) is used to adapt the grid to vortices. However, the present results indicate that helicity does not resolve vortex cores as well as expected, instead it rings the outside, as shown in Figure 5(a).

For configurations such as these that are highly dependent on proper vortex resolution, that is not acceptable, so vorticity ($\vec{\omega}$) was added as an adaption function to *Omnigrid Splitflow*. Vorticity does a much better job of locating the vortex cores, as shown in Figure 5(b) for the same conditions. Note that with no solution adaption, as shown in Figure 5(c), the vortices do not even appear to have been fully formed.

Even at the higher values of α and β, both of these configurations' flow solutions are vortex-dominated. For flows that are transonic or supersonic, vorticity and helicity would not locate the shocks (and often yield a poor or unusable result). In those cases, either gradients of Mach number, gradients of pressure, or divergence of density would most likely be used to refine on compressibility effects. Resolving the flow features is very important, as failure to do so may lead to very different flow solutions.

For flows involving both shocks and shears, some balancing is required; however, most criteria will setup a particular pattern of prioritization, without some sort of weighting that will probably vary from one configuration to another [19]. In some sense, an aerodynamicist is required to have an understanding of the approximate final solution before the computation can be completed. Currently, deciding on the *set* of adaption functions for a given flow is still much more an art than a science.

6.6 Leading Edge Resolution

Traditionally for CFD analysis of lifting surfaces, sufficient leading edge resolution is important. Leading edge resolution is more important for shock-driven flows, or flows where a shock location sets the important results (particularly pitching moment, M_y). These runs are not shock-driven, in particular, but rather vortex driven, and this appears to make LE resolution less significant due to the sharp leading edges. The leading edge resolution is shown in Figure 6 for an ICE configuration at $\alpha = 24°$ and $\beta = 10°$.

This leading edge resolution appears very coarse. Preferably, the grid around the leading edge would be dense enough for the individual grid lines to be indistinguishable at a full-size view for the aircraft. When using *Splitflow* or any comparable unstructured code, a certain amount of "smooth-

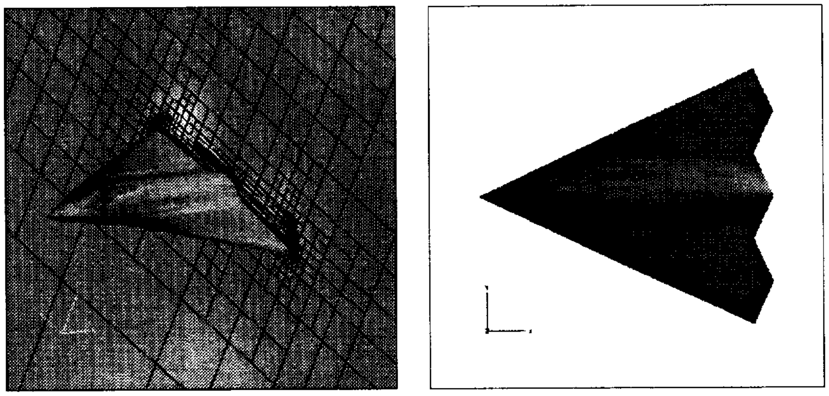

(a) Solution adaption with helicity, $\alpha = 24^\circ, \beta = 10^\circ$

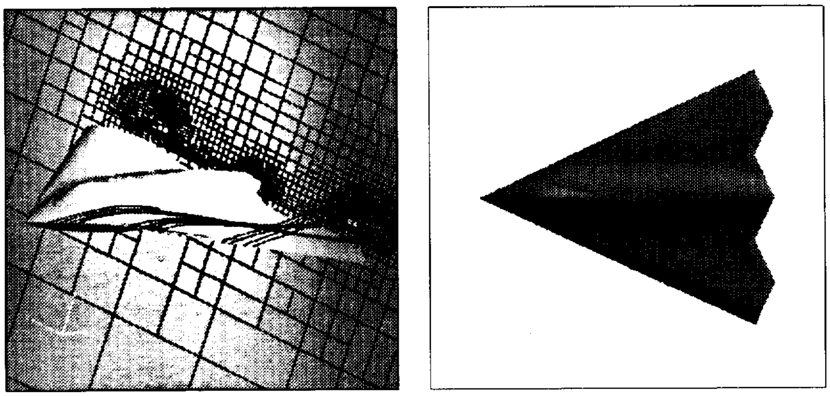

(b) Solution adaption with vorticity, $\alpha = 24^\circ, \beta = 10^\circ$

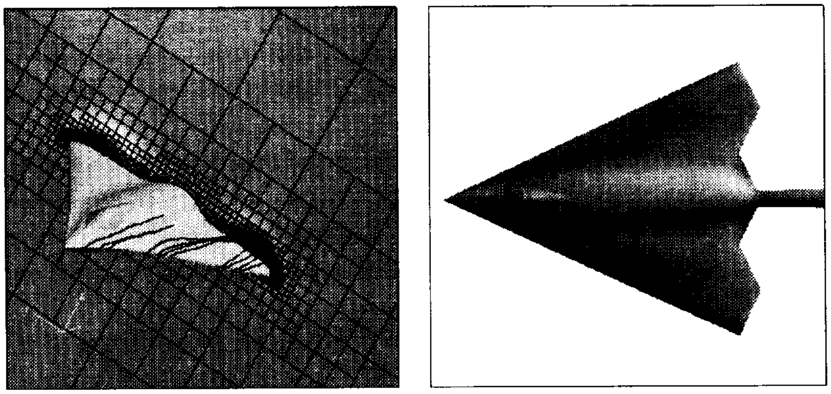

(c) No solution adaption, $\alpha = 24^\circ, \beta = 10^\circ$

Figure 5: Effect of different solution adaption parameters on computed vortex structure

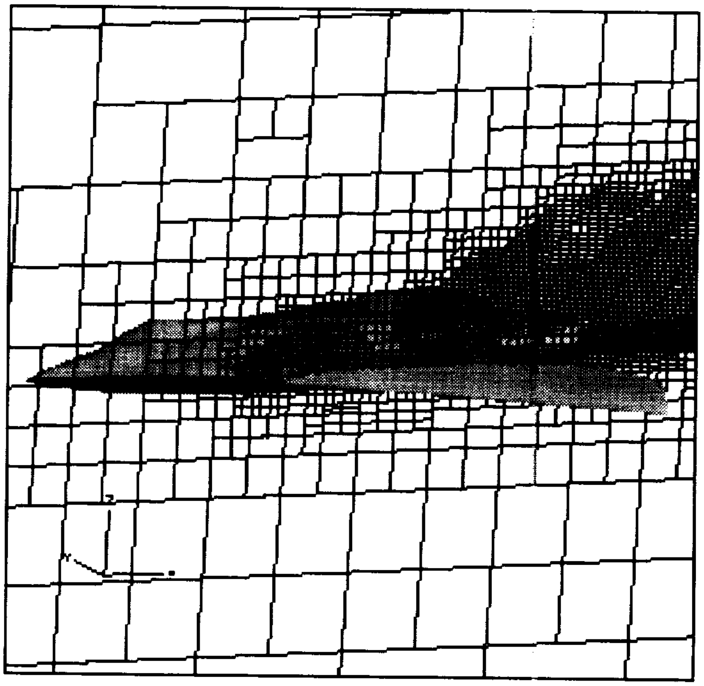

Figure 6: Leading edge resolution for the ICE model

ing" is required to blend the fine-cells near the surface and the larger cells away from the aircraft. In this case, if the cells were that tiny, nearly all of the available cell resources for grid adaption would have been pulled to the leading and trailing edges of the wing leaving nothing left to resolve the vortices without requiring unusably large grid sizes.

6.7 Convergence

Convergence is both a traditional measure and traditional difficulty for the successful use of CFD. Because of the wide range of flow conditions, convergence on some cases was not expected. Further, at higher α (and β?), the expected flow should be unsteady and include significant viscous effects (separation, reattachment, etc.)—under these conditions, a converged Euler solution is probably not expected, and cautious interpretation is required.

For some of these runs, the force and moment coefficients converged well, but convergence was very sensitive to grid adaption. Figure 7 shows the convergence for each of the force and moment coefficients for the typical case $\alpha = 15^\circ$ and $\beta = 5^\circ$. In these cases, some of the values converged well, and others did not. Note also that the same values were reached at moderate and larger grid sizes (greater than 300,000 cells).

Conversely, some of these runs featured very poor convergence properties. Figure 8 shows the force and moment convergence for $\alpha = 30^\circ$ and $\beta = 20^\circ$. Examining these plots, it is not clear that anything is *converging*, much less what it might be converging *towards*.

6.8 Grid Convergence

Grid convergence studies were also performed on certain runs in an effort to determine why certain runs turned out so poorly and if a finer grid would alleviate the problem. While it is unfortunate

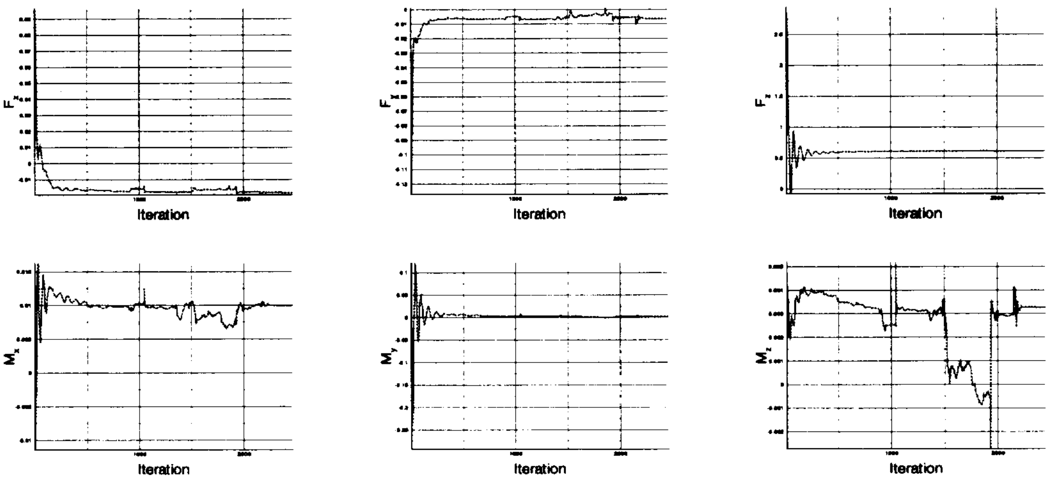

Figure 7: Force/moment convergence, Tailless Delta Wing, $M_\infty = 0.3, \alpha = 15^\circ, \beta = 5^\circ$

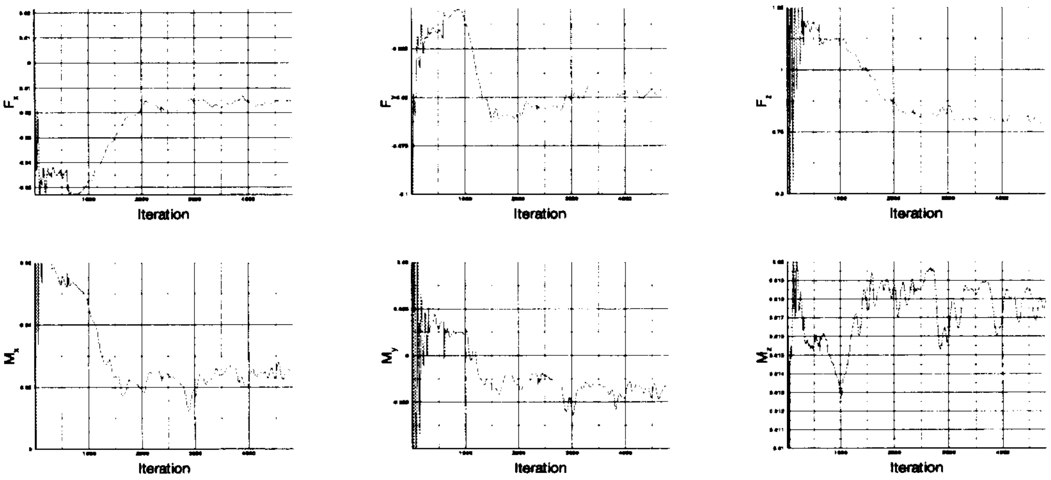

Figure 8: Force/moment "convergence," Tailless Delta Wing, $M_\infty = 0.3, \alpha = 30^\circ, \beta = 20^\circ$

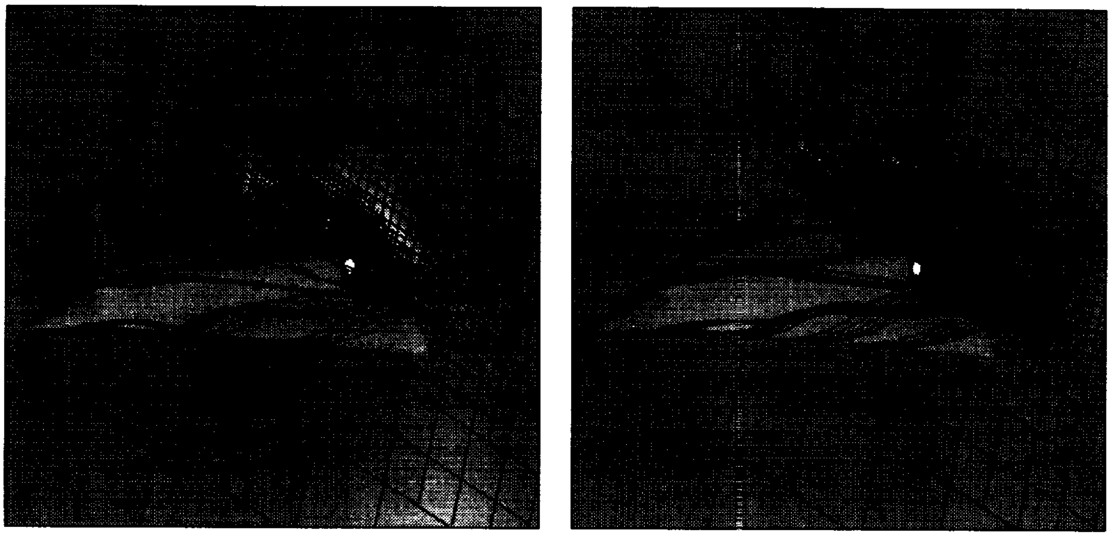

400,000 cells 800,000 cells

Figure 9: Grid convercnce study, ICE model, $\alpha = 24^\circ$, $\beta = 10^\circ$

that the results did not always come into line with the WT data, it is important to point out that a grid converged answer that is far from the experimental data most likely indicates that the physical equation model is not adequate for the problem being considered. Thus, while the results are not what was originally desired, grid convergence to a "wrong" answer provides a very important limit on the applicability of the technique and is useful to its evaluation for problems in that class.

Figure 9 shows a comparison of the converged results for $\alpha = 24^\circ$ and $\beta = 10^\circ$ for approximately 400,000 and 800,000 cells. Note that they generally have the same vortex structure and vorticity pattern (displayed on the aft cutting plane). The larger grid does have "tighter" vortices and a slightly larger recirculation zone on the upwind (right) side

In each case, the computation proceeded to convergence (with respect to the six force and moment coefficients) at both 400,000 and nearly 800,000 cells. As shown in Figure 6.2.3, the computationally predicted pitching moment coefficient is considerably different from the experimentally measured value. In each case, no noticeable improvement was found in matching the WT data.

As these runs progressed, the results were monitored with respect to both convergence of force and moment data and a comparison to provided WT data. The runs presented in this report were declared *done* with either force and moment convergence or for "reasonable time exceeded" (say 4,000 iterations). Since the operational results from this report will be used on future aircraft studies where the tests need to be completed with minimum resources, it is important to determine "how much computation" is required for "good" results. While some cases converged to acceptable results with fewer cells, the method-calibration cases required 400,000 cells before the results consistently matched the WT data. Finally, since 400,000 cells was the minimum required for many cases, and yet no improvement was demonstrated using more cells, this does suggest that 400,000 cells is a useful target grid size for solving this type of problem with *Splitflow*.

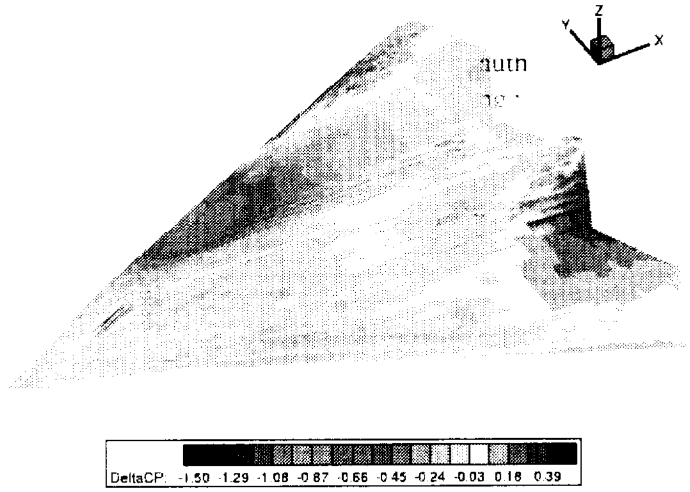

Figure 10: Contour plot of C_p difference, ICE model at $\alpha = 24^\circ, \beta = 10^\circ$

Regrettably, this test is only an approximation to true *grid convergence*. A complete grid convergence test would involve using a sequence of different grids, in particular ones with consistent refinements, to show that the solution obtained is independent of the grid. A final check on this $\alpha = 24^\circ, \beta = 10^\circ$ case involved restarting the similar cases with conditions appropriate for the former:

1. Restarting with the checkpoint solution for $\alpha = 22^\circ, \beta = 10^\circ$, and solving with grid adaption until the forces and moments converged.
2. Restarting with the checkpoint solution for $\alpha = 26^\circ, \beta = 10^\circ$, and solving with grid adaption until the forces and moments converged.
3. Restarting with the checkpoint solution for $\alpha = 22^\circ, \beta = 10^\circ$, and solving *without* grid adaption until the forces and moments converged.

In all three cases, for over 1,000 iterations (and 50 grid adaption cycles where adaption was used!), the computed forces and moments stayed between the values computed for the $\alpha = 22^\circ$ and $\alpha = 26^\circ$ cases, before dropping to a value much closer to that predicted from a dead-start (and far off the wind-tunnel data). While one would like to conclude that some aspect of the grid adaption process is pulling the flow solution away from nature's solution towards a very different one, the fact that the same solution was reached without adapting to the different flow suggests that this "way off" value might be an appropriate solution to the inviscid flow field at these conditions. A contour plot of $\Delta C_p = C_{p_{\mathbf{restart}}} - C_{p_{\mathbf{deadstart}}}$ is shown in Figure 10; one can see the lower pressure on the forward windward "strake" area and the strong higher pressure on the aft-most leeward area—the difference in pitching moment is clear, but this intermediate position is simply not stable.

6.9 CPU Requirements

The inviscid computations presented in this report seemed to take considerably more CPU time than expected. While these numbers are suspicious and being reviewed, a developmental version of *Om-*

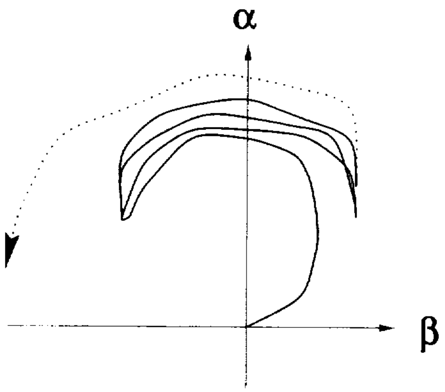

Figure 11: Falling leaf motion

nigrid Splitflow was used for this study; this code has not yet been through a thorough optimization, and this is the first time that this new code has been timed for comparison in this manner.

Since *Omnigrid Splitflow* was designed to run in a parallel environment, it uses a pointwise semi-implicit time marching to advance towards a steady state. It appears that while each iteration may be less computationally expensive, the semi-implicit scheme requires considerably more iterations to advance to a steady state resulting in less efficiency than previously used implicit methods (e.g. *Hybrid Splitflow*).

Contrasting the two codes, while *Omnigrid Splitflow* required $929\mu\mathrm{sec}/(\mathrm{cell}\cdot\mathrm{it})$ for a point-semi-implicit solver, *Hybrid Splitflow* required only $510\mu\mathrm{sec}/(\mathrm{cell}\cdot\mathrm{it})$ for an implicit solver (both times are in Cray J-90 CPU seconds). There is no typical case for the runs presented in this study, but the required number of cells varied from about 300,000 to 400,000, and the required number of iterations was anywhere between 1,500 and 5,000.

In addition to the expense of the flow solver, the runtime was slowed by refining often. Each refinement requires two checkpoint-file writes, plot files, etc. These file operations require an inordinate amount of time on Cray-architecture supercomputers. Certain segments of the refinement process are inherently serial, too, negating some of the strength of both the parallel and vector computers.

In the LMTAS Aerodynamics and CFD computing environment, each run took approximately $40 \sim 130$ "wall clock" hours of runtime. This was on heavily-loaded Cray J-90's, using $4 \sim 8$ processors on a parallel run. Including waiting to get through the queue, each run could take up to one or two weeks.

7 Falling-Leaf Phenomenon

Falling-leaf is a periodically stable flight condition much like a spin. Failling-leaf occurs when the rolling and yawing moments are in-phase and act such that roll encourages yaw and vice versa. Tailless aircraft (such as the ICE and tailless MTVI models discussed herein) are particularly vulnerable to falling-leaf. In falling-leaf motion, the aircraft oscillates rapidly between a high α and small β and a small α and large β ($\alpha \leq 40^\circ, \beta \leq 70^\circ$) as shown in Figure 11. As the aircraft flops back and forth, it resembles a leaf falling through the sky. Hopefully, the aircraft can flop outside the falling-leaf regime so that recovery can be made from this condition and resume normal flight.

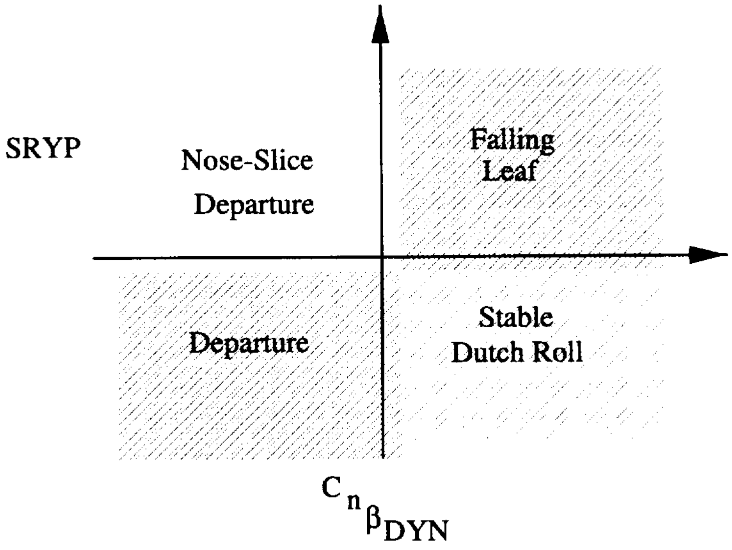

Figure 12: Falling leaf susceptibility region

Falling leaf analysis starts as in [20] with the definition of the Synchronous Roll-Yaw Parameter (SRYP):

$$\text{SRYP} = \frac{\frac{C_{n_\beta}}{C_{l_\beta}} + \frac{I_{xz}}{I_{xx}}}{\frac{I_{zz}}{I_{xx}} + \frac{I_{xz}}{I_{xx}}\frac{C_{n_\beta}}{C_{l_\beta}}} \tag{1}$$

and the Dutch-roll stability parameter:

$$C_{n_{\beta_{\mathrm{DYN}}}} = C_{n_\beta} \cos\alpha - \frac{I_{zz}}{I_{xx}} C_{l_\beta} \sin\alpha \tag{2}$$

where the lateral stability derivative is:

$$C_{l_\beta} = \frac{\partial C_l}{\partial \beta} \simeq \frac{\Delta C_l}{\Delta \beta} \simeq \frac{C_l}{\beta} \tag{3}$$

and the directional stability derivative is:

$$C_{n_\beta} = \frac{\partial C_n}{\partial \beta} \simeq \frac{\Delta C_n}{\Delta \beta} \simeq \frac{C_n}{\beta} \tag{4}$$

given the moments of inertia for the ICE model ($\mathrm{sl} \cdot \mathrm{ft}^2$):

$$I_{xx} = 35,479 \tag{5}$$

$$I_{zz} = 110,627 \tag{6}$$

$$I_{xz} = -525 \tag{7}$$

The falling leaf susceptibility region is defined by:

$$C_{n_{\beta_{\mathrm{DYN}}}} > 0 \quad \bigcap \quad \text{SRYP} > 0 \tag{8}$$

as shown in Figure 12.

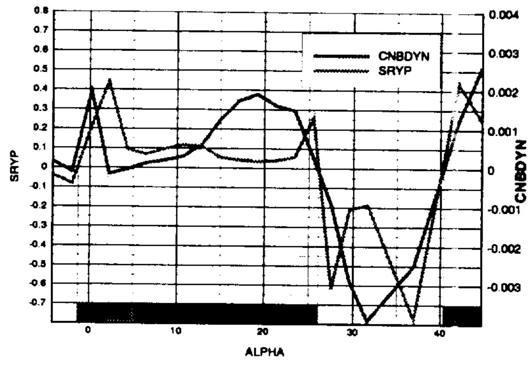

(a) SARL test data

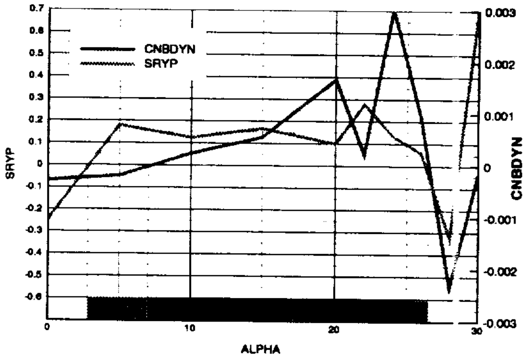

(b) *Splitflow* prediction

Figure 13: Falling leaf results, $\beta = 10^\circ$

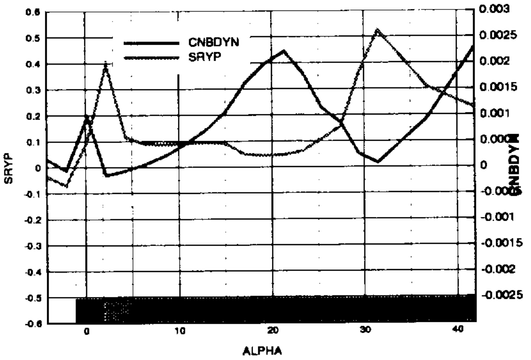

(a) SARL test data

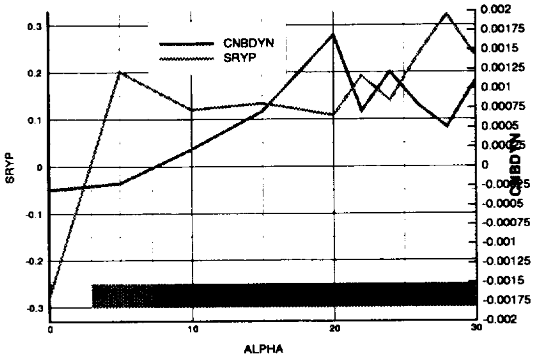

(b) *Splitflow* prediction

Figure 14: Falling leaf results, $\beta = 20^\circ$

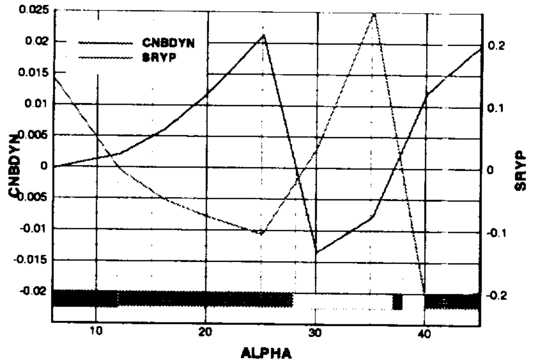

(a) NASA Langley Research Center test data

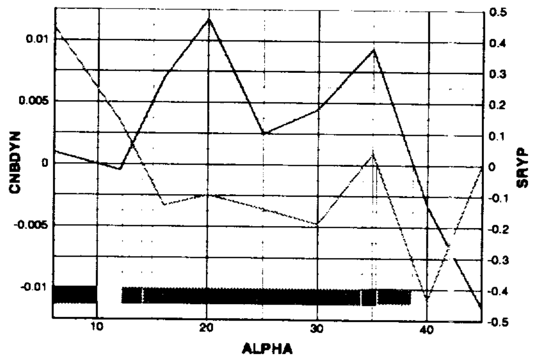

(b) *Splitflow* prediction

Figure 15: Falling leaf results, MTVI, $\beta = 2°$

Falling-leaf results for the tailless delta wing configuration are shown in Figures 13 and 14 for $\beta = 10°$ and $\beta = 20°$ respectively. In the "falling leaf" plots, $C_{n_{\beta_{\mathrm{DYN}}}}$ and SRYP are each plotted with respect to α. Where the curves cross the horizontal zero axis, grey lines are drawn to the bottom. The red (dark) filled areas indicate the region where both parameters remain positive and indicate falling leaf susceptibility (Equation 8). Note that the ranges on the plots of experimental and computational data are different, and when this is considered, the CFD data and wind tunnel data agree very closely.

Finally, results are presented in Figure 15 to show the same falling-leaf analysis for the MTVI model at $\beta = 2°$. Since the moments inertia, I_{xx}, I_{zz}, and I_{xz} were not available, the same moments from the ICE model were used. The results do not look as impressive as the computations on the ICE model, but this is consistent with the differences noted earlier between the ICE and MTVI computations. Note again that the MTVI range included significantly higher angles of attack at which viscous and separation effects are expected to be more significant.

Falling leaf is a natural phenomenon for a tailless (and some tailed) aircraft. Falling leaf is a violent maneuver much like a spin that can result in loss of aircraft and crew. The key to dealing with falling leaf is being both able to avoid it and to recover from an inadvertant entry. One important conclusion from this data is that control augmentation will be required at all α for this class of aircraft—in particular, the use of an active control system will probably be needed to avoid a falling leaf condition. While this report is oriented towards tactical aircraft, other classes of aircraft shaped similarly may also suffer from a tendency towards falling leaf, making this analysis important for non-military aircraft as well (e.g. a flying-wing transport configuration).

8 Conclusions

Much of the desired data can be accurately computed, but often these large nonlinear problems require large grids and longer runtimes than anticipated. At LMTAS, the S&C group desires complete polar analysis in hours, which is not practical with most Euler methods, and Preliminary Design wants a solution per hour, which is definitely not practical today. Also, there were no black boxes here, with each run requiring professional aerodynamic assistance to nurture it to a proper completion.

The problem of how to do rapid aerodynamic predictions for high-performance aircraft design requires more investigation. Several issues are clear:

1. Linear methods do not provide useful data through nonlinear flow regimes.
2. Inviscid methods do not provide useful data through viscous flow regimes.
3. Methods that are fast for one class of problem (e.g. transonic wing/fuselages) may get bogged down on different problems (e.g. high-α delta/wings).
4. It is difficult to incorporate massive computing into the rapid cycle of aircraft design—unless the required data cannot be reasonably obtained otherwise or guessed at.

These problems seem to imply that a fast method is needed for the automatic solution of aerodynamic problems using the Navier-Stokes equations to capture both compressible and viscous effects. Clearly, automatic grid generation and adaptation is still important, as without appropriate grids, the process is doomed. C_L, C_M, and C_{D_0} are critical values, although they can be computed with proper techniques and sufficient patience with the correct physical models. But research needs to proceed in the development of CFD grid generators and flow solvers.

The motivation for this effort is to advance the routine use of CFD in the design of high-performance aircraft by obtaining sufficient accuracy, reducing the time required, and producing codes that are easy to use. While the times required for the simulations presented here are larger than desirable, and effort is still required regarding interface and usability, goal of routine usage of CFD in design is progressing well. Advanced design was already using CFD routinely; along with some of these results regarding using *Splitflow* at high angles of attack and slip, S&C is now starting to use these same methods for concept aircraft derived from the ICE model. Finally, these techniques may be used soon outside of LMTAS to solve related problems in high-performance aircraft design.

8.1 Future Efforts

The Aerodynamics & CFD group at LMTAS is working to develop a completely new version of the *Splitflow* automatic grid generator and flow solver in an effort to easily generate good solutions for either inviscid or viscous analysis. Since numerous difficulties have arisen due to the strangely shaped cells on the surface of the octree grid, the current effort focuses on replacing the *cell cutting* logic with *cell projection.* The goal is to automatically produce tree-like meshes that have smooth near-surface grids suitable for modeling of viscous shear layers. This method represents an attempt to automate the production of a mesh suitable for viscous flow analysis.

Figure 16 shows some of the most recent results from this new code for the ICE model described in this report. The smoother surface mesh is clearly visible, as is the resultant smooth surface pressure contours. While adaptation is currently being implemented in the new code, it should function the same way as the current versions of *Splitflow.*

An advantage of this new method is that the user can now allow adaptation within the viscous shear layers all the way to the surface. A possible disadvantage is that either adaption criteria must be useful in both the off-surface inviscid regions and the near-surface viscous regions, or some method must be created to separate the two.

These grids are also much smoother with respect to neighboring volume ratios, which could often be nearly unbounded with traditional octree methods ($\mathcal{V} \sim 10^{10}$). Meaningless grid parameters such as *body tolerance* have been replaced with physical parameters like *gap size,* and the *sliver cells* that produce cells many orders of magnitude smaller than their neighbors can be eliminated altogether.

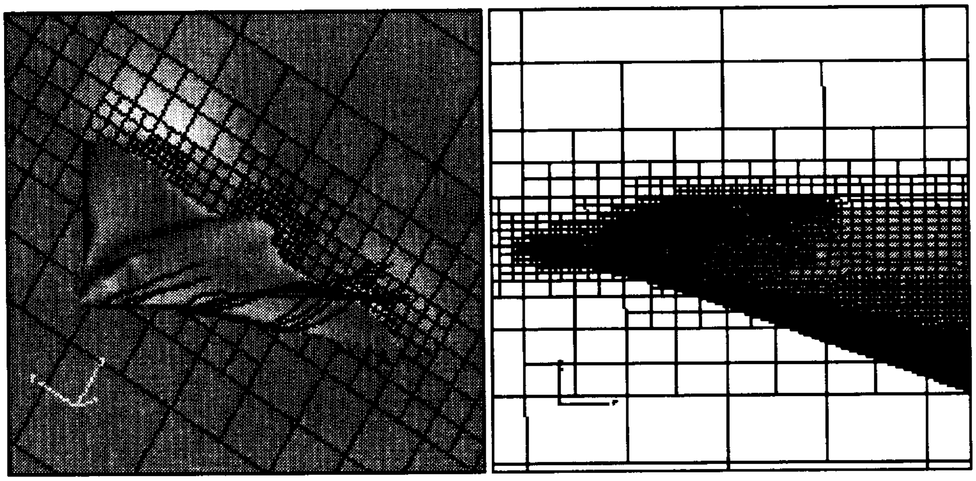

(a) Oblique view

(b) New surface mesh

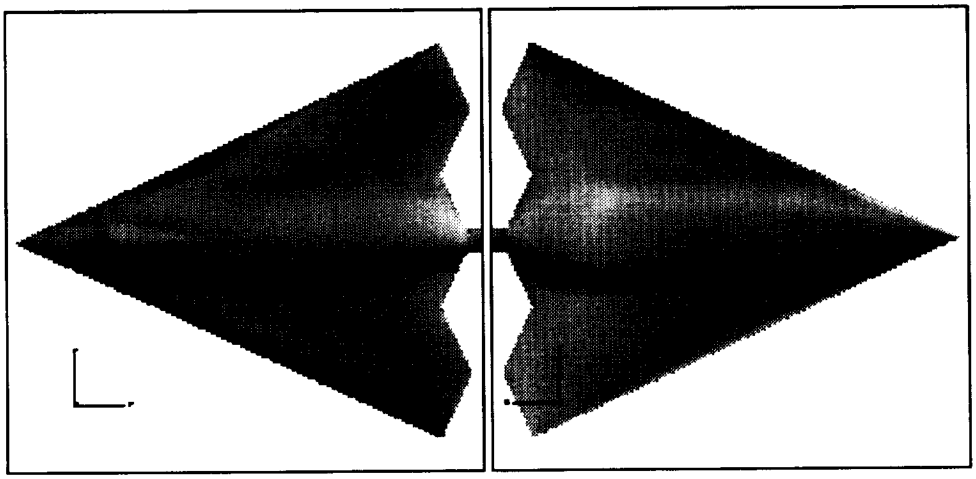

(c) Pressure contours (top)

(d) Pressure contours (bottom)

Figure 16: New grid generation method

9 Acknowledgments

Any large project such as this has many contributors. In particular, the author would like to thank Professor David Darmofal and Dr. Andrew Cary for help in understanding vortex breakdown, Paul McClure from our Advanced Design group, Ken Dorsett from S&C, and Keith Jordan for the surface preparation of both the MTVI and ICE models. *Splitflow* support was provided by Dr. Neal Domel, Dr. Steve Karman, Tracy Welterlen, and Dr. Brian Smith. Finally, both Jim Robarge, the LMTAS program manager, and Farhad Ghaffari, the NASA program manager, were very helpful with oversight and suggestions throughout the program.

References

[1] D. B. Finley, "Euler technology assessment program for preliminary aircraft design employing splitflow code with cartesian unstructured grid method," NASA CR-4649, March 1995.

[2] T. A. Kinard, B. W. Harris, and P. Raj, "An assessment of viscous effects in computational simulation of benign and burst vortex flows on generic fighter wind-tunnel models using team code," NASA CR-4650, March 1995.

[3] D. A. Treiber and D. A. Muilenberg, "Euler technology assessment for preliminary aircraft design employing overflow code with multiblock structured-grid method," NASA CR-4651, March 1995.

[4] D. B. Finley and S. L. Karman, Jr., "Euler technology assessment for preliminary aircraft design - compressibility predictions by employing the cartesian unstructured grid splitflow code," NASA CR-4710, 1996.

[5] T. A. Kinard and P. Raj, "Euler technology assessment for preliminary aircraft design - compressibility predictions by employing the unstructured grid usm3d code," NASA CR-4711, March 1996.

[6] T. A. Kinard, D. B. Finley, and S. L. Karman, Jr., "Prediction of compressibility effects using unstructured euler analysis on vortex dominated flow fields," AIAA 96-2499, June 1996.

[7] J. K. Jordan, "Euler technology assessment—splitflow code applications for stability and control analysis on an advanced fighter model employing innovative control concepts," NASA CR-1998-206943, March 1998.

[8] T. R. Michal, "Euler technology assessment for preliminary aircraft design — unstructured/structured grid NASTD application for aerodynamic analysis of an advanced fighter/tailless configuration," NASA CR-1998-206947, March 1998.

[9] F. Ghaffari, "personal communication," January 1998. NASA Langley Research Center.

[10] A. Beguelin, J. J. Dongarra, G. A. Geist, W. Jiang, R. Manchek, K. Moore, and V. S. Sunderam, "PVM 3 user's guide and reference manual," ORNL TM-12187, May 1993.

[11] B. R. Smith, "The *k-kl* turbulence model and wall layer model for compressible flows," AIAA 90-1483, 1990.

[12] B. R. Smith, "A near wall model for the *k-l* two equation turbulence model," AIAA 94-2386, 1994.

[13] B. R. Smith, "personal communication re: *k-kl* turbulence model." unpublished, July 1998.

[14] M. J. Logan, ed., *Proceedings of the Non-Linear Aero Prediction Requirements Workshop*, March 1994. NASA CP-10138.

[15] S. L. Karman, Jr., *SPLITFLOW User's Manual: Preliminary Copy; Very Rough Draft.* Lockheed Martin Tactical Aircraft Systems, Fort Worth, TX, February 1997.

[16] Amtec Engineering, Inc., P.O. Box 3633, Bellevue, WA 98009-3633, *Tecplot, Interactive Data Visualization for Scientists and Engineers*, 6 ed., 1994.

[17] A. E. Albright, "Modification and validation of conceptual design aerodynamic prediction method HASC95 with VTXCHN," NASA CR-4712, March 1996.

[18] K. M. Dorsett, S. P. Fears, and H. P. Houlden, "Innovative control effectors (ICE) phase II," Wright Laboratory WL-TR-97-3059, August 1997.

[19] E. F. Charlton, *An Octree Solution to Conservation-laws over Arbitrary Regions (OSCAR) with Applications to Aircraft Aerodynamics.* PhD thesis, The University of Michigan, 1997.

[20] J. V. Foster, "Analysis of "falling leaf" motion of class IV airplanes, status update." slides from a talk, July 1995. Flight Dynamics Working Group Meeting, NAWC, Patuxent River, MD.

REPORT DOCUMENTATION PAGE	*Form Approved* *OMB No. 0704-0188*

Public reporting burden for this collection of information is estimated to average 1 hour per response, including the time for reviewing instructions, searching existing data sources, gathering and maintaining the data needed, and completing and reviewing the collection of information. Send comments regarding this burden estimate or any other aspect of this collection of information, including suggestions for reducing this burden, to Washington Headquarters Services, Directorate for Information Operations and Reports, 1215 Jefferson Davis Highway, Suite 1204, Arlington, VA 22202-4302, and to the Office of Management and Budget, Paperwork Reduction Project (0704-0188), Washington, DC 20503.

1. AGENCY USE ONLY *(Leave blank)*

2. REPORT DATE
September 1998

3. REPORT TYPE AND DATES COVERED
Contractor Report

4. TITLE AND SUBTITLE
Numerical Stability and Control Analysis Towards Falling Leaf Prediction Capabilities of Splitflow for Two Generic High-Performance Aircraft Models

5. FUNDING NUMBERS
NAS1-96014, Task 15
WU 522-22-31-01

6. AUTHOR(S)
Eric F. Charlton

7. PERFORMING ORGANIZATION NAME(S) AND ADDRESS(ES)
Lockheed-Martin Tactical Aircraft Systems
Fort -Worth, TX 76101

8. PERFORMING ORGANIZATION REPORT NUMBER

9. SPONSORING/MONITORING AGENCY NAME(S) AND ADDRESS(ES)
National Aeronautics and Space Administration
Langley Research Center
Hampton, VA 23681-2199

10. SPONSORING/MONITORING AGENCY REPORT NUMBER
NASA/CR-1998-208730

11. SUPPLEMENTARY NOTES
This study was performed by Lockheed-Martin Tactical Aircraft Systems under subcontract to Lockheed-Martin Engineering & Sciences, Hampton Virginia under contract to NASA Langley Research Center.
Langley Technical Monitor: Mr. Farhad Ghaffari

12a. DISTRIBUTION/AVAILABILITY STATEMENT
Unclassified-Unlimited
Subject Category 2 Distribution: Standard
Availability: NASA CASI (301) 621-0390

12b. DISTRIBUTION CODE

13. ABSTRACT *(Maximum 200 words)*

Aerodynamic analysis are performed using the Lockheed-Martin Tactical Aircraft Systems (LMTAS) Splitflow computational fluid dynamics code to investigate the computational prediction capabilities for vortex-dominated flow fields of two different tailless aircraft models at large angles of attack and sideslip. These computations are performed with the goal of providing useful stability and control data to designers of high performance aircraft. Appropriate metrics for accuracy, time, and ease of use are determined in consultations with both the LMTAS Advanced Design and Stability and Control groups. Results are obtained and compared to wind-tunnel data for all six components of forces and moments. Moment data is combined to form a "falling leaf" stability analysis. Finally, a handful of viscous simulations were also performed to further investigate nonlinearities and possible viscous effects in the differences between the accumulated inviscid computational and experimental data.

14. SUBJECT TERMS
Computational Fluid Dynamics, Euler/Navier-Stokes, Preliminary Aircraft Design, Falling-Leaf Phenomenon, Vortical Flows, Cartesian/Unstructured-Grid Splitflow

15. NUMBER OF PAGES
59

16. PRICE CODE
A04

17. SECURITY CLASSIFICATION OF REPORT	18. SECURITY CLASSIFICATION OF THIS PAGE	19. SECURITY CLASSIFICATION OF ABSTRACT	20. LIMITATION OF ABSTRACT
Unclassified	Unclassified	Unclassified	

NSN 7540-01-280-5500

Standard Form 298 (Rev. 2-89)
Prescribed by ANSI Std. Z-39-18
298-102